nature Accelerated Article Preview

LETTER
doi:10.1038/nature25179

Selective silencing of euchromatic L1s revealed by genome–wide screens for L1 regulators

Nian Liu, Cameron H. Lee, Tomek Swigut, Edward Grow, Bo Gu, Michael Bassik & Joanna Wysocka

Cite this article as: Liu, N. *et al.* Selective silencing of euchromatic L1s revealed by genome-wide screens for L1 regulators. *Nature* http://dx.doi.org/10.1038/nature25179 (2017).

Received 15 May; accepted 28 November 2017.
Accelerated Article Preview Published online 6 December 2017.

LETTER

doi:10.1038/nature25179

Selective silencing of euchromatic L1s revealed by genome–wide screens for L1 regulators

Nian Liu[1]*, Cameron H. Lee[2]*, Tomek Swigut[1], Edward Grow[2,7], Bo Gu[1], Michael Bassik[2,3] & Joanna Wysocka[1,4,5,6]

Transposable elements (TEs) are now recognized not only as parasitic DNA, whose spread in the genome must be controlled by the host, but also as major players in genome evolution and regulation[1–6]. Long INterspersed Element-1 (LINE-1 or L1), the only currently autonomous mobile transposon in humans, occupies 17% of the genome and continues to generate inter- and intra-individual genetic variation, in some cases resulting in disease[1–7]. Nonetheless, how L1 activity is controlled and what function L1s play in host gene regulation remain incompletely understood. Here, we use CRISPR/Cas9 screening strategies in two distinct human cell lines to provide the first genome-wide survey of genes involved in L1 retrotransposition control. We identified functionally diverse genes that either promote or restrict L1 retrotransposition. These genes, often associated with human diseases, control the L1 lifecycle at transcriptional or post-transcriptional levels and in a manner that can depend on the endogenous L1 sequence, underscoring the complexity of L1 regulation. We further investigated L1 restriction by MORC2 and human silencing hub (HUSH) complex subunits MPP8 and TASOR[8]. HUSH/MORC2 selectively bind evolutionarily young, full-length L1s located within transcriptionally permissive euchromatic environment, and promote H3K9me3 deposition for transcriptional silencing. Interestingly, these silencing events often occur within introns of transcriptionally active genes and lead to down-regulation of host gene expression in a HUSH/MORC2-dependent manner. Together, we provide a rich resource for studies of L1 retrotransposition, elucidate a novel L1 restriction pathway, and illustrate how epigenetic silencing of TEs rewires host gene expression programs.

Most of our knowledge about L1 retrotransposition control comes from studies examining individual candidate genes[2–6]. To systematically identify genes regulating L1 retrotransposition, we performed a genome-wide CRISPR/Cas9 screen in human chronic myeloid leukemia K562 cells using an L1-G418^R retrotransposition reporter[9] (Fig. 1a,b). Importantly, the L1-G418^R reporter was modified to be driven by a doxycycline (dox)-responsive promoter, as opposed to the native L1 5'UTR, to avoid leaky retrotransposition ahead of the functional screen (Extended Data Fig. 1a-c). The cells become G418^R antibiotic resistant only when the L1-G418^R reporter undergoes a successful retrotransposition event following dox-induction (Fig. 1b). For the screen, we transduced clonal L1-G418^R cells with a lentiviral genome-wide sgRNA library such that each cell expressed a single sgRNA[10]. We then dox-induced the cells to turn on the L1-G418^R reporter for retrotransposition, and split the cells into G418-selected conditions and unselected conditions, which served to eliminate cell growth bias in the screen analysis. The frequencies of sgRNAs in the two populations were measured by deep sequencing (Fig. 1a) and analyzed using Cas9 high-Throughput maximum Likelihood Estimator (CasTLE)[11]. Consequently, cells transduced with sgRNAs targeting L1 suppressors would have more retrotransposition events than negative control cells and would be enriched through the G418 selection; conversely, cells transduced with sgRNAs targeting L1 activators would be depleted.

Using the above strategy, we identified 25 putative L1 regulators at a 10% FDR cutoff, and 150 genes at a 30% FDR cutoff (Fig. 1c and Extended Data Fig. 1d; see Table S1 for full list). Despite low statistical confidence, many of the 30% FDR cutoff genes overlapped previously characterized L1 regulators (e.g. ALKBH1, SETDB1) and genes functioning in complexes with our top 10% FDR hits (e.g. Fanconi Anemia pathway, HUSH complex), suggesting that they likely encompassed biologically relevant hits. To increase statistical power in distinguishing bona fide L1 regulators among these, we performed a high-coverage secondary screen targeting the 30% FDR hits (150 genes) and an additional 100 genes that were either functionally related to our top hits or which were otherwise previously known to regulate L1 but fell outside of the 30% FDR cutoff threshold (See Table S2 for full list). This secondary screen validated 90 genes out of the top 150 genome-wide screen hits, a fraction close to expected with the 30% FDR cutoff (Fig. 1d and Extended Data Fig. 2a-c).

Altogether, our two-tier screening approach identified 142 human genes that either activate or repress L1 retrotransposition in K562 cells, encompassing over 20 previously known L1 regulators (Extended Data Fig. 2d). Novel candidates are involved in functionally diverse pathways, such as chromatin/transcriptional regulation, DNA damage/repair, and RNA processing (Extended Data Fig. 2e,f). While many DNA damage/repair factors, particularly the Fanconi Anemia (FA) factors, suppress L1 activity, genes implicated in the Non-Homologous End Joining (NHEJ) repair pathway promote L1 retrotransposition (Extended Data Fig. 2f). In agreement, mutations in some of the identified NHEJ factors were previously found to result in decreased retrotransposition frequencies[12]. Intriguingly, many hits uncovered by our screen (e.g. FA factors, MORC2 and SETX) are associated with human disorders[13–17].

To extend our survey of L1 regulators to another cell type, we performed both a genome-wide and a secondary screen in HeLa cells (Extended Data Fig. 1b, 1e) with the same sgRNA libraries used in the K562 screens. Importantly, top hits identified in the K562 genome-wide screen were recapitulated in the HeLa screen (e.g. MORC2, TASOR, SETX, MOV10) (Extended Data Fig. 3a). Furthermore, secondary screens in both K562 and HeLa cells showed concordant effects for groups of genes, for example, the suppressive effects of the FA complex genes, and activating effects of the NHEJ pathway genes (Extended Data Fig. 3b-e). Interestingly, however, a subset of genes showed cell-line selective effects (Extended Data Fig. 3c). At the same time, some of the previously known L1 regulators did not come up as hits in our

[1]Department of Chemical and Systems Biology, Stanford School of Medicine, Stanford University, Stanford, CA 94305, USA. [2]Department of Genetics, Stanford School of Medicine, Stanford University, Stanford, CA 94305, USA. [3]Stanford University Chemistry, Engineering, and Medicine for Human Health (ChEM-H), Stanford School of Medicine, Stanford University, Stanford, CA 94305, USA. [4]Institute of Stem Cell Biology and Regenerative Medicine, Stanford School of Medicine, Stanford University, Stanford, CA 94305, USA. [5]Department of Developmental Biology, Stanford School of Medicine, Stanford University, Stanford, CA 94305, USA. [6]Howard Hughes Medical Institute, Stanford School of Medicine, Stanford University, Stanford, CA 94305, USA. [7]Present address: Huntsman Cancer Institute, University of Utah, Salt Lake City, UT 841125550, USA.
*Co-first author

screen. Several factors could have limited our ability to identify all genes controlling L1 retrotransposition to saturation, such as: (i) a subset of regulators may function in a cell-type specific manner not captured by either K562 or HeLa screens, (ii) essential genes with strong negative effects on cell growth may have dropped out, (iii) regulators that strictly require native L1 UTR sequences may have been missed due to our reporter design. Nonetheless, our combined screens identify many novel candidates for L1 retrotransposition control in human cells and provide a rich resource for mechanistic studies of TEs.

Select screen hits were further validated in K562 cells using a well-characterized L1-GFP reporter[18] (Extended Data Fig. 1a), confirming 13 suppressors and 1 activator (SLTM) out of 16 examined genes (Fig. 1e). Interestingly, chromatin regulators (TASOR, MORC2, MPP8, SAFB and SETDB1) suppress the retrotransposition of L1-GFP reporter, but not that of a previously described codon-optimized L1-GFP reporter (hereinafter referred to as (opt)-L1-GFP)[19,20], indicating that these factors regulate L1 retrotransposition in a manner dependent upon the native L1 ORF nucleotide sequence (Extended Data Fig. 3f,g). An additional secondary screen against the codon-optimized (opt)-L1-G418^R reporter in K562 cells confirmed the sequence-dependent feature of these L1 regulators, and systematically partitioned our top screen hits into native L1 sequence-dependent and –independent candidates (Extended Data Fig. 3h, see Table S2 for full list).

We next examined whether the identified regulators influence the expression of endogenous L1Hs, the youngest and only retrotransposition-competent L1 subfamily in humans. CRISPR-deletion of some genes (TASOR, MPP8, SAFB and MORC2) significantly increased expression of endogenous L1Hs, whereas deletion of other genes, such as SETX, RAD51 or FA complex components, had little effect (Fig. 1f). Since all interrogated genes restrict L1-GFP retrotransposition into the genome (Fig. 1e and Extended Data Fig. 4a), our results suggest that identified suppressors can function at either transcriptional or posttranscriptional level.

We further investigated three candidate transcriptional regulators of L1: MORC2, TASOR and MPP8. TASOR and MPP8 (along with PPHLN1), comprise the HUSH complex and recruit the H3K9me3 methyltransferase SETDB1 to repress genes[8]. Notably, PPHLN1 and SETDB1 also came up as L1 suppressors in our screen (Fig. 1d and Extended Data Fig. 3b). MORC2, which has recently been shown to biochemically and functionally interact with HUSH[21], is a member of the microrchidia (MORC) protein family that has been implicated in transposon silencing in plants and mice[22,23]. While MORC2/HUSH have been previously implicated in heterochromatin formation, most heterochromatin factors had no impact on L1 retrotransposition, suggesting a selective effect (Fig. 2a and Extended Data Fig. 4b).

Several independent experiments in clonal knockout (KO) K562 lines confirmed that HUSH and MORC2 suppress the retrotransposition of the L1-GFP reporter by silencing its transcription (Fig. 2b,c and Extended Data Fig. 4c-f). Additionally, HUSH/MORC2 repressed endogenous (non-reporter) L1Hs RNA and protein expression in both K562 and human embryonic stem cells[24] (hESC, H9) (Fig. 2d and Extended Data Fig. 4g-k). PolyA-selected RNA sequencing (RNA-seq) experiments revealed up-regulated expression of evolutionarily younger L1PA families (including L1Hs) upon HUSH or MORC2 KO in K562 cells (Fig. 2e). Taken together, these data demonstrate that HUSH/MORC2 silence both the reporter transgene as well as endogenous evolutionarily young L1s.

Chromatin immunoprecipitation followed by sequencing (ChIP-seq) from K562 cells and hESCs demonstrated that MORC2, MPP8 and TASOR co-bind genomic regions characterized by specific L1 instances. Elements from the primate-specific L1P family showed higher enrichment than the older L1M family elements (Fig. 3a,b and Extended Data Fig. 5a,b, 7a,b), consistent with the preferential derepression of the former upon HUSH or MORC2 KO (Fig. 2e). Moreover, this enrichment was specific to L1s, as other major repeat classes were not enriched (Fig. 3b and Extended Data Fig. 7b), although all three proteins also targeted expressed KRAB-ZNF genes (Extended Data Fig. 5c,d). HUSH KO in K562 cells almost completely abrogated MORC2 binding at L1s (consistent with recently published observations that HUSH recruits MORC2 for transcriptional repression[21]), whereas MORC2 deletion led to a modest, but appreciable decrease of HUSH subunit binding (Extended Data Fig. 6). In mouse ESCs, MPP8 bound retrotransposition-competent L1Md-A and L1Md-T, as well as IAP elements, a class of murine endogenous retroviruses that remain currently mobile in the mouse genome (Extended Data Fig. 7c,d), suggesting that regulators uncovered by our study in human cells may in other species target additional active transposons beyond L1s.

Interestingly, even within younger human L1Ps only a subset is bound by HUSH/MORC2 in either K562 cells or hESCs, and we sought to identify genomic or epigenomic features that could explain this selectivity. We found that HUSH/MORC2 selectively target young full-length L1s, particularly the L1PA1-5 in human cells (Fig. 3c,d) and L1Md-A/T in mice (Extended Data Fig. 7e). Both MPP8 and MORC2 bind broadly across the L1; while MORC2 binding is skewed towards the 5' end, MPP8 shows higher enrichments within the body and at 3' end of L1PAs, including the L1Hs (L1PA1) elements (Extended Data Fig. 7f,g).

Nonetheless, preference for the full-length, evolutionarily younger L1PAs can only partially explain observed HUSH/MORC2 selectivity, as only a subset of such elements is targeted by the complex (Fig. 3d). We found that the additional layer of selectivity can be explained by the state of surrounding chromatin, with HUSH/MORC2-occupied L1s preferentially immersed within the transcriptionally permissive euchromatic environment marked by modifications such as H3K4me3 and H3K27ac (Fig. 3e). In agreement, HUSH/MORC2-bound L1s are enriched within introns of actively transcribed genes (Extended Data Fig. 8a,b). Furthermore, although most HUSH/MORC2-bound L1s are concordant between K562 and hESCs, those that are bound in a cell type-specific manner tend to be associated with genes that are differentially active between the two cell types (Extended Data Fig. 8c). To understand the role of transcription in HUSH/MORC2 targeting of L1s, we investigated MORC2 and MPP8 occupancy at the inducible L1 transgene. We observed increased binding of these factors upon transcriptional induction (Extended Data Fig. 8d), suggesting that transcription through L1 sequences facilitates HUSH/MORC2 binding. Taken together, HUSH/MORC2 selectively target young, full-length L1s located within transcriptionally permissive euchromatic regions, which are precisely the elements that pose the highest threat to genome integrity, as a subset of them remains mobile and transcription is the first step of L1 mobilization.

Despite their immersion within the euchromatic environment, HUSH/MORC2-bound L1s themselves are heavily decorated with the transcriptionally repressive H3K9me3 (Fig. 3e), consistent with the role of HUSH in facilitating H3K9me3 deposition at target sites[8]. HUSH/MORC2 KO decreased H3K9me3 level preferentially at L1 versus non-L1 HUSH/MORC2 genomic targets, and at bound versus unbound L1s (Fig. 4a and Extended Data Fig. 9a,b). Since HUSH/MORC2-bound L1s are significantly enriched within introns of transcriptionally active genes (Extended Data Fig. 8a-c), we examined whether HUSH/MORC2 recruitment and its associated H3K9me3 deposition can influence chromatin modification and expression of the host genes. Despite the transcriptionally active status (Extended Data Fig. 8a,b), promoters and especially bodies of genes harboring MORC2/HUSH-bound L1s show appreciable levels of H3K9me3. This enrichment is substantially diminished in the KO lines (Extended Data Fig. 9c) with the concomitant upregulation of genes harboring MORC2/HUSH-bound L1s, but not those with unbound intronic L1s (Fig. 4b). Thus, HUSH/MORC2 binding at intronic L1s leads to a modest, but significant down-regulation of the active genes that harbor them (Fig. 4c and Extended Data Fig. 9d-g, 10a).

Inserting L1 sequences on a transcript leads to decrease in RNA expression via inadequate transcript elongation,[25] and this effect has been attributed to the A/T enrichment of L1s. However, our results argue that transcriptional attenuation of host gene expression could be a consequence of epigenetic silencing by HUSH/MORC2 (Fig. 4b,c and Extended Data Fig. 9d-g, 10a), and this possibility is consistent with the described role of genic H3K9me3 in decreasing Pol II elongation rate, leading to its accumulation over the H3K9me3 region[26]. If such mechanism is at play, then HUSH KO should decrease accumulation of the elongating Pol II over L1 bodies, and this is indeed what we observe in Pol II ChIP-seq experiments (though interestingly, at 5' UTRs of L1s, Pol II levels are relatively elevated in the KOs) (Extended Data Fig. 10b).

Importantly, host gene regulation is directly dependent on the presence of the intronic L1, as deletion of select MORC2/HUSH-bound L1s from the intron led to the upregulation of host mRNA to a level commensurate with the magnitude of changes caused by HUSH/MORC2 KO (Fig. 4d,e and Extended Data Fig. 10c,d). Thus, dampening expression levels of an active gene can be a by-product of a retrotransposition event and associated HUSH/MORC2-mediated L1 silencing (Fig. 4f). Although observed effects on active host genes are only modulatory, they occur to various extents at hundreds of human genes, illustrating how TE activity can rewire host gene expression patterns.

Online Content Methods, along with any additional Extended Data display items and Source Data, are available in the online version of the paper; references unique to these sections appear only in the online paper.

Received 15 May; accepted 28 November 2017.
Published online 6 December 2017.

1. Lander, E. S. *et al.* Initial sequencing and analysis of the human genome. *Nature* **409**, 860–921 (2001).
2. Levin, H. L. & Moran, J. V. Dynamic interactions between transposable elements and their hosts. *Nat. Rev. Genet.* **12**, 615–627 (2011).
3. Beck, C. R., Garcia-Perez, J. L., Badge, R. M. & Moran, J. V. LINE-1 Elements in Structural Variation and Disease. *Annu. Rev. Genomics Hum. Genet.* **12**, 187–215 (2011).
4. Mita, P. & Boeke, J. D. How retrotransposons shape genome regulation. *Curr. Opin. Genet. Dev.* **37**, 90–100 (2016).
5. Goodier, J. L. Restricting retrotransposons: a review. *Mob. DNA* **7**, 16 (2016).
6. Chuong, E. B., Elde, N. C. & Feschotte, C. Regulatory activities of transposable elements: from conflicts to benefits. *Nat. Rev. Genet.* **18**, 71–86 (2017).
7. Philippe, C. *et al.* Activation of individual L1 retrotransposon instances is restricted to cell-type dependent permissive loci. *eLife* **5**, e13926 (2016).
8. Tchasovnikarova, I. A. *et al.* Epigenetic silencing by the HUSH complex mediates position-effect variegation in human cells. *Science* **348**, 1481–1485 (2015).
9. Moran, J. V. *et al.* High Frequency Retrotransposition in Cultured Mammalian Cells. *Cell* **87**, 917–927 (1996).
10. Morgens, D. W. *et al.* Genome-scale measurement of off-target activity using Cas9 toxicity in high-throughput screens. *Nat. Commun.* **8**, 15178 (2017).
11. Morgens, D. W., Deans, R. M., Li, A. & Bassik, M. C. Systematic comparison of CRISPR-Cas9 and RNAi screens for essential genes. *Nat. Biotechnol.* **34**, 634–636 (2016).
12. Suzuki, J. *et al.* Genetic Evidence That the Non-Homologous End-Joining Repair Pathway Is Involved in LINE Retrotransposition. *PLoS Genet.* **5**, (2009).
13. Chance, P. F. *et al.* Linkage of the gene for an autosomal dominant form of juvenile amyotrophic lateral sclerosis to chromosome 9q34. *Am. J. Hum. Genet.* **62**, 633–640 (1998).
14. Németh, A. H. *et al.* Autosomal Recessive Cerebellar Ataxia with Oculomotor Apraxia (Ataxia-Telangiectasia–Like Syndrome) Is Linked to Chromosome 9q34. *Am. J. Hum. Genet.* **67**, 1320–1326 (2000).
15. Albulym, O. M. *et al.* MORC2 mutations cause axonal Charcot–Marie–Tooth disease with pyramidal signs. *Ann. Neurol.* **79**, 419–427 (2016).
16. Schottmann, G., Wagner, C., Seifert, F., Stenzel, W. & Schuelke, M. MORC2 mutation causes severe spinal muscular atrophy-phenotype, cerebellar atrophy, and diaphragmatic paralysis. *Brain* **139**, e70–e70 (2016).
17. Brégnard, C. *et al.* Upregulated LINE-1 Activity in the Fanconi Anemia Cancer Susceptibility Syndrome Leads to Spontaneous Pro-inflammatory Cytokine Production. *EBioMedicine* **8**, 184–194 (2016).
18. Ostertag, E. M., Luning Prak, E. T., DeBerardinis, R. J., Moran, J. V. & Kazazian, H. H. Determination of L1 retrotransposition kinetics in cultured cells. *Nucleic Acids Res.* **28**, 1418–1423 (2000).
19. Han, J. S. & Boeke, J. D. A highly active synthetic mammalian retrotransposon. *Nature* **429**, 314–318 (2004).
20. Wagstaff, B. J., Barnerβoi, M. & Roy-Engel, A. M. Evolutionary Conservation of the Functional Modularity of Primate and Murine LINE-1 Elements. *PLOS ONE* **6**, e19672 (2011).
21. Tchasovnikarova, I. A. *et al.* Hyperactivation of HUSH complex function by Charcot-Marie-Tooth disease mutation in MORC2. *Nat. Genet.* **49**, 1035–1044 (2017).
22. Moissiard, G. *et al.* MORC Family ATPases Required for Heterochromatin Condensation and Gene Silencing. *Science* **336**, 1448–1451 (2012).
23. Pastor, W. A. *et al.* MORC1 represses transposable elements in the mouse male germline. *Nat. Commun.* **5**, 5795 (2014).
24. Garcia-Perez, J. L. *et al.* LINE-1 retrotransposition in human embryonic stem cells. *Hum. Mol. Genet.* **16**, 1569–1577 (2007).
25. Han, J. S., Szak, S. T. & Boeke, J. D. Transcriptional disruption by the L1 retrotransposon and implications for mammalian transcriptomes. *Nature* **429**, 268–274 (2004).
26. Saint-André, V., Batsché, E., Rachez, C. & Muchardt, C. Histone H3 lysine 9 trimethylation and HP1γ favor inclusion of alternative exons. *Nat. Struct. Mol. Biol.* **18**, 337–344 (2011).
27. Khan, H., Smit, A. & Boissinot, S. Molecular evolution and tempo of amplification of human LINE-1 retrotransposons since the origin of primates. *Genome Res.* **16**, 78–87 (2006).

Supplementary Information is available in the online version of the paper.

Acknowledgements We thank J. Moran for the LRE-GFP plasmid and Astrid Engel for the codon-optimized L1 construct. We thank D. Fuentes, A. Spencley, R. Srinivasan, J. Mohammed, V. Bajpai, K. Tsui, G. Hess, D. Morgens, G. Cornelis for assistance and discussions. We thank K. Cimprich, A. Fire, A. Urban for comments on the manuscript. This work was funded by Jane Coffin Childs Memorial Fund for Medical Research (N.L.), NSF DGE-114747 (C.H.L.), NIH R01HG008150 (M.C.B.), NIH 1DP2HD084069-01 (M.C.B.), NIH R01 GM112720 and Howard Hughes Medical Institute grants (J.W.).

Author Contributions N.L., C.L., T.S., J.W., M.B. designed and performed experiments, analyzed data and wrote the manuscript. E.G., C.L., J.W., M.B. initiated the K562 genome-wide screen. B.G. analyzed smFISH data. J.W., M.B. supervised the entire work.

Author Information Reprints and permissions information is available at www.nature.com/reprints. The authors declare no competing financial interests. Readers are welcome to comment on the online version of the paper. Publisher's note: Springer Nature remains neutral with regard to jurisdictional claims in published maps and institutional affiliations. Correspondence and requests for materials should be addressed to J.W. (wysocka@stanford.edu) or M.B. (bassik@stanford.edu).

Reviewer Information *Nature* thanks D. Bourch'his and the other anonymous reviewer(s) for their contribution to the peer review of this work.

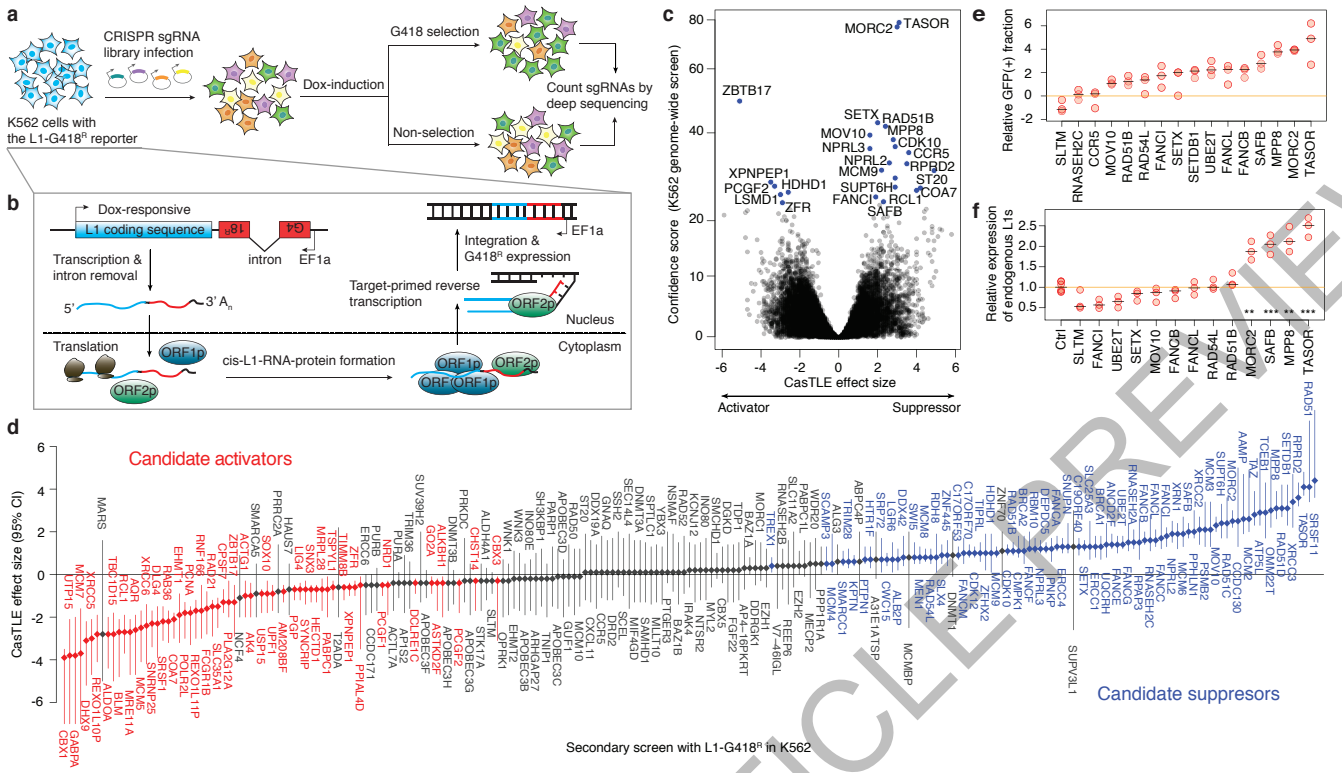

Figure 1 | Genome-wide screen for L1 activators and suppressors in K562 cells. a. Schematic for the screen. b. Schematic for the L1-G418^R retrotransposition. c. CasTLE analysis of (n = 2) independent K562 genome-wide screens. Genes at 10% FDR cutoff colored in blue, CasTLE likelihood ratio test[11]. d. The maximum effect size (center value) estimated by CasTLE from two independent K562 secondary screens with 10 independent sgRNAs per gene. Bars, 95% credible interval (CI). L1 activators, red; L1 suppressors, blue; insignificant genes whose CI include 0, gray. e. L1-GFP retrotransposition in control (infected with negative control sgRNAs, hereinafter referred to as 'Ctrl') and mutant K562 cells as indicated. GFP(+) cell fractions normalized to Ctrl. Center value as median. n = 3 biological replicates per gene. f. RT-qPCR measuring endogenous L1Hs expression in mutant K562 cells, normalized to Ctrl. Center value as median. n = 3 technical replicates per gene. **P < 0.01; ***P < 0.001; two-sided Welch t-test.

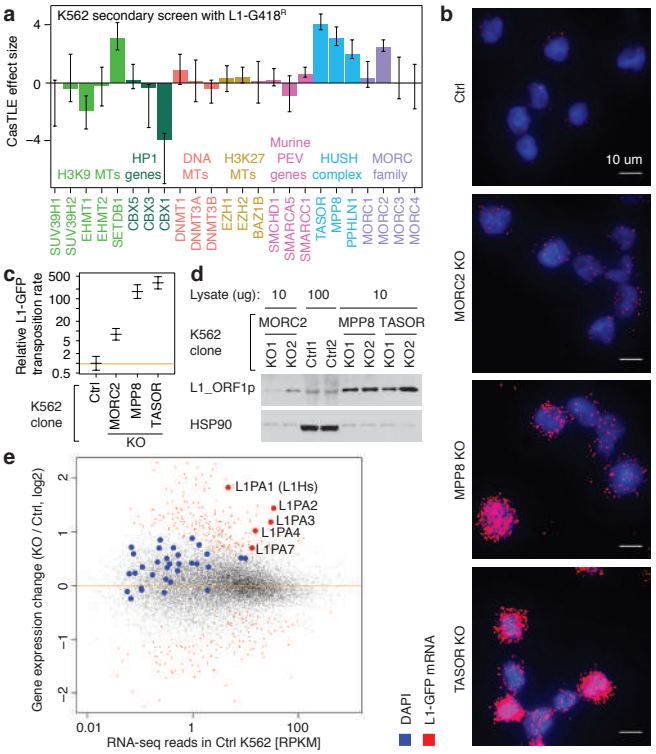

Figure 2 | HUSH and MORC2 silence L1 transcription to inhibit retrotransposition. a. The maximum effect size (center value) of indicated heterochromatin regulators, estimated by CasTLE from two independent K562 secondary screens with 10 independent sgRNAs per gene. Error bars, 95% credible intervals. b. Visualization of L1-GFP mRNAs in dox-induced K562 clones, from single smFISH experiment that was independently repeated twice with similar results. See also Extended Data Fig. 4d,e. c. L1-GFP retrotransposition rate[18] (center value) in K562 clones, from logistic regression fit of the GFP(+) cell counts at 7 time points (0, 5, 10, 15, 20, 25, 30 days post-induction) and two independent clones per gene. Over 200 GFP(+) cells per cell count. Data normalized to Ctrl. Bar, 95% credible interval. d. Endogenous L1_ORF1p level in K562 clones by western blots, HSP90 as loading control. Three experiments repeated independently with similar results. e. RNA-seq read counts from MORC2 KO, MPP8 KO and TASOR KO K562 clones, compared to Ctrl RNA-seq reads. n = 6 + 2 biologically independent RNA-seq experiments). Dots represent transcripts; large dots represent L1 transcripts. Red, significant changes (padj < 0.1, DESeq analysis); blue and gray, insignificant changes.

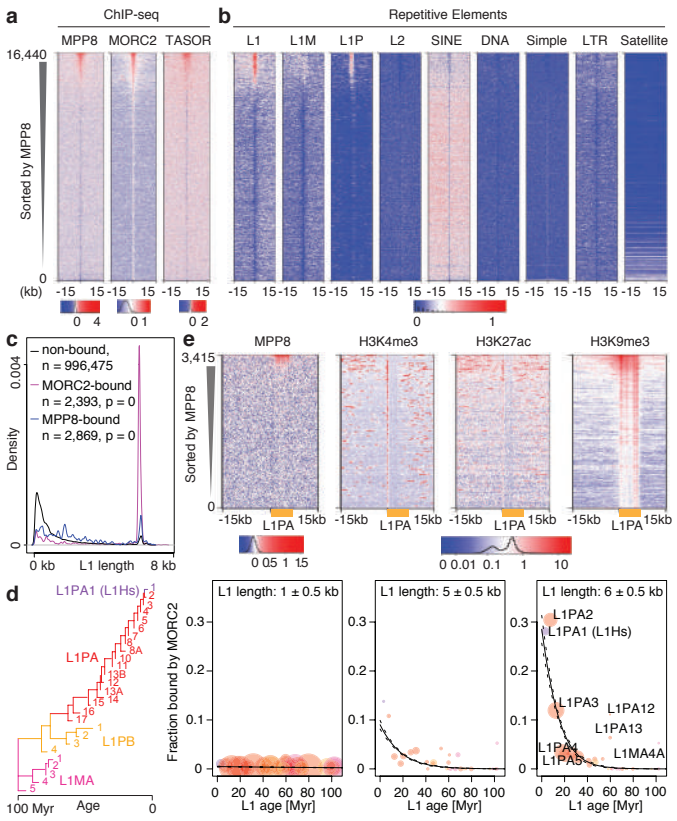

Figure 3 | HUSH/MORC2 target young full-length L1s in euchromatic environment. a. Heatmaps showing signal enrichment of ChIPs with indicated antibodies in K562 cells, sorted by MPP8 ChIP signal and centered on MPP8 and MORC2 peaks. Plotted is normalized ChIP signal (Ctrl subtracted with corresponding KO). b. Heatmaps showing MPP8 and MORC2 ChIP signal enrichment over repetitive elements, centered and sorted as in (a). c. Size distribution of the L1s bound or unbound by MORC2 or MPP8 in K562 cells. P-values, two-tailed Kolmogorov-Smirnov test. d. Fraction of MORC2–bound L1s (center values) as function of L1 length (three size classes are presented) and age (predicted from the phylogenetic analysis[27]) in K562 cells. Colored circles represent L1 families, with areas proportional to count of L1 instances with indicated age and length. n = 1,501 MORC2–bound L1 + 200,160 unbound L1. $p = 2.2 \times 10^{-90}$ for age–length interaction term, lower for simple terms (ANOVA, χ^2 test), plotted logistic regression lines with 95% credible interval. e. Heatmaps showing signal enrichment of ChIPs with indicated antibodies in K562 cells, centered on the 5' end of full-length L1PAs.

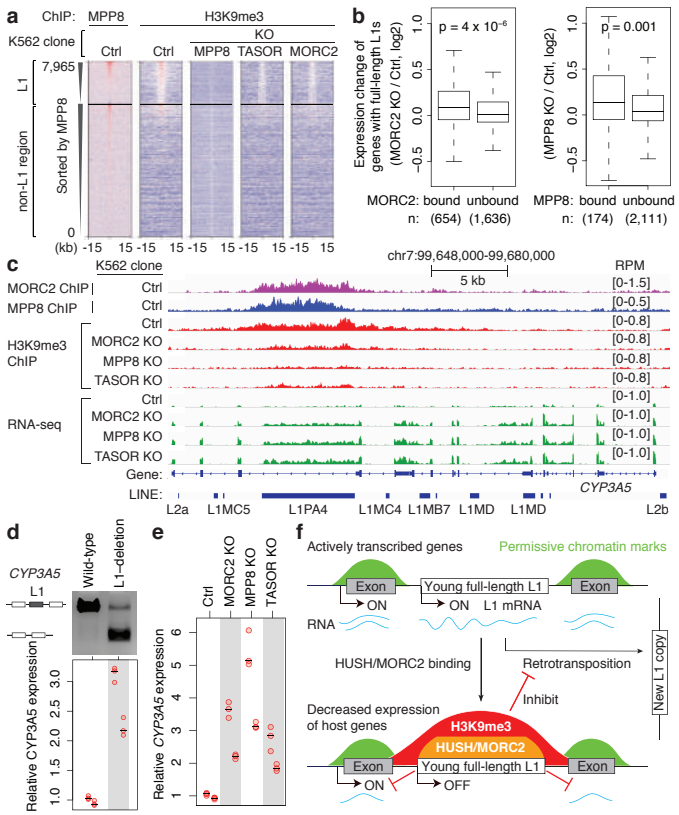

Figure 4 | HUSH/MORC2 binding at L1s decreases active host gene expression. a. Heatmaps showing MPP8 and H3K9me3 ChIP signal enrichment, centered on MPP8 and MORC2 summits and separated by L1 presence or absence. b. Expression change of genes with intronic full-length L1s that are bound or unbound by MORC2 or MPP8 (RNA-seq reads from KO K562 clones compared to Ctrl). Box plots show median and interquartile range (IQR), whiskers are 1.5× IQR. p-value, two-sided Mann-Whitney-Wilcoxon test. c. Genome browser tracks: HUSH/MORC2 loss causing H3K9me3 decrease at the target L1 and expression increase at both the target L1 and its host gene, independently repeated once with similar results. d. Deleting the target intronic L1 from *CYP3A5* in K562 increases *CYP3A5* expression, by RT-qPCR normalized to wild-type sample. n = 2 biological replicates x 3 technical replicates (center value as median). Gel image confirms L1 deletion; two experiments repeated independently with similar results. e. RT-qPCR for *CYP3A5* expression in K562 clones, normalized to Ctrl. n = 2 biological replicates x 3 technical replicates (center value as median). f. Model: HUSH/MORC2 bind young full-length L1s within transcriptionally active genes, and promote H3K9me3 deposition at target L1s to silence L1 transcription. This pathway not only inhibits L1 retrotransposition, but also decreases host gene expression.

METHODS

Cell culture and antibodies. K562 cells (ATCC) were grown in Roswell Park Memorial Institute (RPMI) 1640 Medium (11875093, Life Technologies) supplemented with 10% Fetal Bovine Serum (Fisher, Cat# SH30910), 2 mM L-glutamine (Fisher, Cat# SH3003401) and 1% penicillin-streptomycin (Fisher, Cat#SV30010), and cultured at 37 °C with 5% CO_2. HeLa cells (ATCC) were grown in Dulbecco's Modified Eagle's Medium (Life Technologies, Cat# 11995073) supplemented with 10% FBS, 2 mM L-glutamine, and 1% penicillin-streptomycin, and cultured at 37 °C with 5% CO_2. H9 human ES cells were expanded in feeder-free, serum-free medium mTeSR-1 from StemCell technologies, passaged 1:6 every 5–6 days using accutase (Invitrogen) and re-plated on tissue culture dishes coated overnight with growth-factor-reduced matrigel (BD Biosciences). Male mouse embryonic stem cells (R1) were grown as described[28]. Cell cultures were routinely tested and found negative for mycoplasma infection (MycoAlert, Lonza).

Rabbit MORC2 antibody (A300-149A, Bethyl Laboratories), Rabbit MPP8 antibody (16796-1-AP, Protein Technologies Inc), Rabbit TASOR antibody (HPA006735, Atlas Antibodies) were used in Western blots (1:1000 dilution) and ChIP assays. Mouse anti-LINE-1 ORF1p antibody (MABC1152, Millipore)[29], Rabbit HSP90 (C45G5, Cell Signalling, #4877), Beta actin antibody (ab49900, Abcam) were used in Western blots. Histone H3 (tri-methyl K9) antibody (ab8898, Abcam) and RNA Pol II (Santa Cruz Biotechnology, N-20 sc-899) were used in ChIP assays.

L1 reporters. The L1-ORF1-ORF2 sequence is derived from the LRE-GFP[30], a gift from John Moran. To make the L1-GFP reporter, we used Gibson assembly to clone the L1_ORF1/2 fragment and a GFP-B-globin-intron cassette driven by the mammalian promoter EF1a into the pB transgene using a dox inducible promoter (modified from PBQM812A-1, System Biosciences) to drive the L1 sequence and a UBC-RTTA3-ires Blast as a selectable marker for reporter integration. To make the L1-G418^R reporter, we replaced the GFP-B-globin-intron fragment in the L1-GFP reporter with a NEO-intron-NEO cassette driven by the mammalian promoter EF1a. The codon-optimized L1-ORF1-ORF2 sequence in our (opt)-L1 reporter is derived from the SynL1_optORF1_neo, a gift from Astrid Engel[31]. We replaced the self-splicing Tetrahymena NEO-intron-NEO cassette with the neo-B-globin-intron-neo cassette driven by the EF1a promoter or the GFP-B-globin-intron-GFP cassette driven by the EF1a promoter. This L1-syn-ORF1-ORF2-indicator cassette was inserted into the pB transgene using a dox inducible promoter and a UBC-RTTA3-ires Blast, as described above.

Genome-wide screen in K562 cells. The K562 cell line (with a BFP-Cas9 lentiviral transgene) was nucleofected with the pB-tetO-L1-G418^R/Blast construct and the piggyBac transposase (PB210PA-1, System Biosciences) following the manufacturer's instructions (Lonza 2b nucleofector, T-016 program). The nucleofected cells were sorted using limiting dilution in 96-well plates, and positive clones were screened first for sensitivity to Blast, and then the ability to generate G418 resistant cells after dox induction. The Cas9/L1-G418^R cells were lentivirally infected with a genome-wide sgRNA library as described[10], containing ~200,000 sgRNAs targeting 20,549 protein-coding genes and 13,500 negative control sgRNAs at an MOI of 0.3-0.4 (as measured by the mCherry fluorescence from the lentiviral vector), and selected for lentiviral integration using puromycin (1 μg/ml) for 3 days as the cultures were expanded for the screens. In duplicate, 200x10^6 library-infected cells were dox-induced (1 μg/ml) for 10 consecutive days, with a logarithmic growth (500k cells/ml) maintained each day of the dox-induction. After dox-induction, the cells were recovered in normal RPMI complete media for 24 hours, and then split into the G418-selection condition (300 μg/ml G418, Life Technologies, Cat# 11811031) and non-selection conditions. After 7 days of maintaining cells at 500k/ml, 200 M cells under each condition were recovered in normal RPMI media for 24 hours, before they were pelleted by centrifugation for genomic DNA extraction using Qiagen DNA Blood Maxi kit (Cat# 51194) as described[32]. The sgRNA-encoding constructs were PCR-amplified using Agilent Herculase II Fusion DNA Polymerase (Cat# 600675) (See **Table S4** for the primer sequences used). These libraries were then sequenced across two Illumina NextSeq flow cells (~40 M reads per condition; ~200x coverage per library element). Computational analysis of genome-wide screen was performed as previously described[10,11] using CasTLE, which is a maximum likelihood estimator that uses a background of negative control sgRNAs as a null model to estimate gene effect sizes. See **Table S1** for the K562 genome-wide screen results.

Secondary screen in K562 cells. The secondary screen library included the following, non-comprehensive sets of genes (253 genes in total, ~10 sgRNAs per gene, plus 2500 negative control sgRNAs): all genes falling within ~30% FDR from the K562 genome-wide screen (~150 genes), genes known to be functionally related to the 30% FDR genes, genes previously implicated in L1 biology, and genes involved in epigenetic regulation or position effect variegation (see **Table S2** for a complete list). The library oligos were synthesized by Agilent Technologies and cloned into pMCB320 using BstXI/BlpI overhangs after PCR amplification. The Cas9/L1-G418^R (or Cas9/(opt)-L1-G418^R) K562 cell line was lentivirally infected with the secondary library (~4,500 elements) at an MOI of 0.3-0.4 as described previously[33]. After puromycin selection (1 μg/ml for 3 days) and expansion, 40 M (~9,000 coverage per library element) cells were dox-induced for 10 days in replicate, recovered for 1 day, and split for 7-day G418-selection and non-selection conditions, with a logarithmic growth (500k cells/ml) maintained as in the K562 genome-wide screen. 10M cells under each condition were used for genomic extractions, sequenced (~6-10M reads per condition; ~1000-2000x coverage per library element) and analyzed using casTLE as described above[10,11]. See **Table S2** for the K562 secondary screen results with L1-G418^R and (opt)-L1-G418^R.

Genome-wide screen and Secondary screen in HeLa cells. The pB-tetO-L1-G418^R/Blast construct was integrated into Cas9 expressing HeLa cells with piggyBac transposase via nucleofection (Lonza 2b nucleofector, I-013 program) following the manufacturer's instructions. The Cas9/L1-G418^R HeLa cells were blasticidin (10 μg/ml) selected, screened for sensitivity to G418 and the ability to generate G418 resistance cells after dox induction, and lentivirally infected with the genome-wide sgRNA library or with the secondary sgRNA library. Infected cells were then puromycin selected (1 μg/ml) for 5 days and expanded for the screens.

For the genome-wide screen, ~200x10^6 Cas9/L1-G418^R HeLa cells (~1,000x coverage of sgRNA library) were dox-induced for 10 days in replicate, recovered for 1 day, and split for 8-day G418-selection and non-selection conditions, with cells being split every other day to maintain the sgRNA library at a minimum of ~350x coverage. ~200M (1,000x coverage) cells per condition were used for genomic extractions and sequencing as described above for the K562 screens. See **Table S1** for the HeLa genome-wide screen results.

For the secondary screen, ~1x10^7 Cas9/L1-G418^R HeLa cells (~2,000x coverage of sgRNA library) were dox-induced for 10 days in replicate, recovered for 1 day, and split for 8-day G418-selection and non-selection conditions, with cells being split every other day to maintain ~400x coverage. ~5 million (1,000x coverage) cells per condition were used for genomic extractions and sequencing as described above. See **Table S2** for the HeLa secondary screen results.

Validation of individual candidates using the L1-GFP retrotransposition assay. To validate the genome-wide screen hits, we infected clonal Cas9/L1-GFP K562 cells with individual sgRNAs as previously described[32], 3 independent mutant cell lines per gene, each with a different sgRNA (cloned into pMCB320 using BstXI/BlpI overhangs; mU6:sgRNA; EF1a:Puromycin-t2a-mCherry). See **Table S3** for sgRNA sequences. The infected cells were selected against puromycin (1 μg/ml) for 3 days, recovered in fresh RPMI medium for 1 day, and dox-induced for 10 days. Then, the percentage of GFP(+) cells was measured on a BD Accuri C6 Flow Cytometer (GFP fluorescence detected in FL1 using 488 nm laser) after gating for live mCherry(+) cells.

CRISPR-mediated deletion of individual genes and intronic L1s. To delete genes in H9 ESCs, we cloned target sgRNAs in pSpCas9(BB)-2A-GFP (PX458) as described[34]. The sgRNA plasmids were prepared with the Nucleospin plasmid kit (Macherey Nagel) and transfected into H9 ESCs using Fugene following the manufacturer's instructions. After 48-72 hrs, GFP-positive transfected cells were sorted and expanded. Gene depletion effects were validated by western blots.

To delete the L1 from the host gene intron, we designed sgRNAs targeting both upstream and downstream side of the L1 within the intron; one was cloned into pSpCas9(BB)-2A-BFP, while the other into pSpCas9(BB)-2A-GFP. The two sgRNA plasmids were mixed at 1:1 ratio and nucleofected into K562 cells via electroporation following the manufacturer's instructions. After 48-72 hours, BFP/GFP-positive transfected cells were single-cell sorted and expanded. The genetic deletion effects were validated by PCR assay.

Western blotting. Live cells were lysed for 30 min at 4 °C in protein extraction buffer (300 mM NaCl, 100 mM Tris pH 8, 0.2 mM EDTA, 0.1% NP40, 10% glycerol) with protease inhibitors and centrifuged to collect the supernatant lysate. The cell lysate was measured with Bradford reagent (Biorad), separated on SDS-PAGE gels and transferred to nitrocellulose membranes. The L1-reporter containing K562 cells had not been dox-induced when used for western blot assays characterizing endogenous L1_ORF1p levels (Fig. 2d and Extended Data Fig. 4k).

PCR and gel electrophoresis. PCR experiments characterizing the L1-G418^R retrotransposition and the deletion of intronic L1s were performed with Phusion High-Fidelity DNA Polymerase (M0530S, NEB), following the manufacturer's instructions. In general, 30 cycles of PCR reactions were performed at an annealing temperature 5 °C below the Tm of the primer. No 'spliced' PCR products can be detected without dox-induction, even with 40 PCR cycles. PCR reaction products were separated on 1% agarose gels with ethidium bromide. Primer sequences are in **Table S4**.

qRT-PCR and PspGI-assisted qPCR. Total RNA was isolated from live cells using the RNeasy kit (74104, Qiagen) and treated with RNase-Free DNase Set (79254, Qiagen) to remove genomic DNA, according to the manufacturer's instructions. 500 ng total RNA was reverse transcribed with SuperScriptA III First-Strand Synthesis System (18080051, Life Technologies) following the manufacturer's instructions. Beta-actin mRNA was used as internal control within each RNA sample (Figs. 1f and 4d,e). The sequences of PCR primers, including the one targeting the 5'UTR of L1Hs[35–37], are summarized in **Table S4**.

Genomic DNA was isolated using PureLink Genomic DNA Mini Kit (K182001, Life Technologies) with RNase A digestion to remove contaminant RNA, according to the manufacturer's instructions. 300 ng genomic DNA per sample was digested with 50 units PspGI (R0611S, New England Biolabs) in 1x smart buffer (NEB) at 75 °C for 1hr, to cut uniquely at the intron of the GFP cassette. The reaction mixture was then used in qPCR experiments with primers flanking the intron in the GFP cassette (**Table S4**). Due to the PspGI digestion, the original unspliced L1-GFP reporter will not be amplified by PCR. Only newly integrated GFP cassettes, where the intron was removed during the retrotransposition process, can be PCR amplified. qPCR runs and analysis were performed on the Light Cycler 480II machine (Roche).

Northern Blotting. Northern blotting was conducted as previously described[38]. Briefly, 15 μg of total RNA from K562 cells or H9 ESC cells was separated on the 0.7% formaldehyde agarose gel, capillary transferred overnight in 20x SSC to the Hybond N membrane (GE Healthcare), crosslinked with a Stratalinker (Stratagene), and hybridized with ^{32}P-labeled single-stranded DNA probes (10^6 cpm/ml) in ULTRAhyb-Oligo Hybridization Buffer (AM8663, Life Technologies) following the manufacturer's instructions. Blots were washed two times with wash buffer (2X SSC, 0.5%SDS), and then exposed to film overnight to several days at −80 °C with an intensifying screen. The sequence of oligonucleotide probes is in **Table S3**.

Single molecule FISH. Single molecule FISH (smFISH) assays were performed following the affymetrix Quantigene ViewRNA ISH Cell Assay user manual. 2.5-5 million live K562 cells were fixed within 4% formaldehyde in 1x PBS for 60 mins at RT, resuspended in 1x PBS, pipetted onto poly-L-lysine coated glass cover slip (∼20,000 total cells/spot; spread out with a pipette tip), and baked in dry oven at 50±1 °C for 30 minutes to fix the cells onto the glass slip, followed by digestion with Protease QS (1:4000) in 1x PBS for 10 minutes at RT. Cells were hybridized with smFISH probes, designed to target beta actin mRNA (FITC channel) and the L1-GFP reporter mRNA (Cy3 channel), DAPI stained for 5 mins, and mounted with Prolong Gold Antifade Reagent (10 ml/sample). Images were taken by spinning disk confocal microscope equipped with 60x 1.27NA water immersion objective with an effective pixel size of 108x108 nm. Specifically, for each field of view, a z-series of 8 μm is taken with 0.5 μm/z-step for all 3 channels. For quantitation, maximum-projected images from the z-series is used and analyzed by a custom-written matlab script. In brief, all images are first subtracted with the background determined with the OTSU method[39] from the log-transformed image after pillbox blurring with a radius of 3 pixels. mRNA puncta are segmented by tophat filter using the background subtracted images and only the ones above 25th percentile intensity of all segmented puncta are taken for downstream analysis. Each punctum is then assigned to the nuclear mask identified by image areas above the previously determined background. For each single cell, the assigned pixel area of L1-GFP mRNA is then normalized to the assigned pixel area of beta-actin mRNA per cell.

RNA-seq. Two independent biological replicates of K562 cells in culture were extracted to isolate DNA-free total RNA sample, using the RNeasy kit (74104, Qiagen) combined with the RNase-Free DNase Set (79254, Qiagen). PolyA-selected RNA were isolated using 'Dynabeads mRNA Purification Kit for mRNA Purification from Total RNA preps' (610-06, Life Technologies) following the manuals. 100 ng polyA-selected RNA was fragmented with NEBNext Magnesium RNA Fragmentation Module (E6150S, New England Biolabs), and used for first strand cDNA synthesis with SuperScriptII (18064-014, Invitrogen) and random hexamers, followed by second strand cDNA synthesis with RNAseH (18021-014, Invitrogen) and DNA PolI (18010-025, Invitrogen). The cDNA was purified, quantified, multiplexed and sequenced with 2x 75bp pair-end reads on an Illumina NEXT-seq (Stanford Functional Genomics Facility).

RNA-seq reads were aligned to hg38 reference genome with hisat2 (--no-mixed, --no-discordant) without constraining to known transcriptome. Known (gencode 25) and de-novo transcript coverages were quantified with featureCount. Repeat Masker coverage was quantified with bedtools coverage. Reads mapping to the same repeat family were then tabulated together, since individual read coverage was too low to obtain meaningful results. Differential expression analysis of join gene-repeat data was performed with DESeq2[40].

ChIP-seq. Two replicates of ChIP experiments per sample were performed as previously described[41,42]. Approximately 0.5–1 × 10^7 cells in culture per sample were crosslinked with 1% paraformaldehyde (PFA) for 10 min at room temperature (RT), and quenched by 0.125 M glycine for 10 min at RT. Chromatin was sonicated to an average size of 0.2-0.7 kb using a Covaris (E220 evolution). Sonicated chromatin was incubated with 5-10 μg antibody bound to 100 μl protein G Dynabeads (Invitrogen) and incubated overnight at 4 °C, with 5% kept as input DNA. Chromatin was eluted from Dynabeads after five times wash (50 mM Hepes, 500 mM LiCl, 1 mM EDTA, 1% NP-40, 0.7% Na-deoxycholate), and incubated at 65 °C water bath overnight (12-16 hrs) to reverse crosslinks. ChIP DNA were subject to end repair, A-tailing, adaptor ligation and cleavage with USER enzyme, followed by size selection to 250-500 bp and amplification with NEBNext sequencing primers. Libraries were purified, quantified, multiplexed (with NEBNext Multiplex Oligos for Illumina kit, E7335S) and sequenced with 2x 75 bp pair-end reads on an Illumina NEXT-seq (Stanford Functional Genomics Facility).

ChIP-seq reads were trimmed with cutadapt (-m 50 -q 10) and aligned with bowtie2 (version 2.2.9, --no-mixed --no-discordant --end-to-end -maxins 500) to the hg38 reference genome. ChIP peaks were called with macs2 (version 2.1.1.20160309) callpeak function with broad peak option and human genome effective size using reads form corresponding loss of gene lines as background model. Visualization tracks were generated with bedtools genomecov (-bg -scale) with scaling factor being 10^6/number aligned reads and converted to bigWig with bedGraphToBigWig (Kent tools). BigWigs were plotted with IGV browser. Individual alignments were inspected with IGB browser.

Heatmaps were generated by intersecting bam alignment files with intervals of interest (bedtools v2.25.0), followed by tabulation of the distances of the reads relative to the center of the interval and scaling to account for total aligned read numbers (10^6/number aligned). Heatmaps were plotted using a custom R function. Aggregate plots were generated by averaging rows of the heatmap matrix. For ChIPs in Ctrl and KO K562 clones, ChIP-seq signals in the corresponding KO cells were used as the null reference.

For ChIP-seq repetitive sequence relationship analysis, repeat masker was intersected with ChIP-seq peak calls to classify each masker entry as MPP8 bound, MORC2-bound or unbound. Enriched families of repeats were identified with R fisher.test() followed by FDR correction with qvalue(). Distribution of sizes of occupied vs non-occupied L1 was plotted using R density() with sizes being taken from repeat masker. ks.test() was used to reject null hypothesis that distribution of sizes for bound and unbound L1s is the same. To investigate relationship between L1 age, length and occupancy, logistic regression was performed with R glm() engine.

Quantitative analysis of H3K9me3 changes was performed by first identifying regions of significant enrichment in each sample relative to corresponding input sample (macs2 callpeak), merging the intervals into a common superset. This superset was joined with a decoy randomized set of intervals, twice the size of actual experimental interval set, with the same size distribution (bedtools shuffle). Next the read coverage was determined for each sample (bedtools coverage) and regions with significant change together with fold changes were identified using DESeq2[40]. H3K9me3 regions were classified into bound vs unbound by performing intersect with MORC2 and MPP8 ChIP peak calls.

Data availability. All sequencing data generated in this work has been deposited at GEO under the accession number: GSE95374. H3K4me3 and H3K27ac K562 ChIP-seq datasets in Fig. 3e are from BioProject (accession number PRJEB8620). hESC RNA-seq datasets in Extended Data Fig. 8c are from SRA run entries SRR2043329 and SRR2043330. The complete results of genome-wide screens in K562 and HeLa cells are in Table S1; The complete results of secondary screens in K562 and HeLa cells are in Table S2. The sequences of gRNAs and oligonucleotides used in this work are in Table S3 and Table S4. The uncropped scans with size marker indications are summarized in the Supplementary Figure. All data are available from the corresponding author upon reasonable request.

Code availability. Detailed Data and further code information are available on request from the authors.

28. Buecker, C. *et al.* Reorganization of Enhancer Patterns in Transition from Naive to Primed Pluripotency. *Cell Stem Cell* **14**, 838–853 (2014).
29. Taylor, M. S. *et al.* Affinity proteomics reveals human host factors implicated in discrete stages of LINE-1 retrotransposition. *Cell* **155**, 1034–1048 (2013).
30. Brouha, B. *et al.* Evidence Consistent with Human L1 Retrotransposition in Maternal Meiosis I. *Am. J. Hum. Genet.* **71**, 327–336 (2002).
31. Gasior, S. L., Roy-Engel, A. M. & Deininger, P. L. ERCC1/XPF limits L1 retrotransposition. *DNA Repair* **7**, 983–989 (2008).
32. Deans, R. M. *et al.* Parallel shRNA and CRISPR-Cas9 screens enable antiviral drug target identification. *Nat. Chem. Biol.* **12**, 361–366 (2016).
33. Bassik, M. C. *et al.* A Systematic Mammalian Genetic Interaction Map Reveals Pathways Underlying Ricin Susceptibility. *Cell* **152**, 909–922 (2013).
34. Cong, L. *et al.* Multiplex Genome Engineering Using CRISPR/Cas Systems. *Science* **339**, 819–823 (2013).
35. Coufal, N. G. *et al.* L1 Retrotransposition in Human Neural Progenitor Cells. *Nature* **460**, 1127–1131 (2009).
36. Shukla, R. *et al.* Endogenous Retrotransposition Activates Oncogenic Pathways in Hepatocellular Carcinoma. *Cell* **153**, 101–111 (2013).
37. Carreira, P. E. *et al.* Evidence for L1-associated DNA rearrangements and negligible L1 retrotransposition in glioblastoma multiforme. *Mob. DNA* **7**, (2016).
38. Doucet, A. J., Wilusz, J. E., Miyoshi, T., Liu, Y. & Moran, J. V. A 3′ Poly(A) Tract Is Required for LINE-1 Retrotransposition. *Mol. Cell* **60**, 728–741 (2015).
39. Otsu, N. A Threshold Selection Method from Gray-Level Histograms. *IEEE Trans. Syst. Man Cybern.* **9**, 62–66 (1979).
40. Love, M., Huber, W. & Anders, S. Moderated estimation of fold change and dispersion for RNA-seq data with DESeq2. *Genome Biol.* **15**, 550 (2014).
41. Bajpai, R. *et al.* CHD7 cooperates with PBAF to control multipotent neural crest formation. *Nature* **463**, 958–962 (2010).
42. Rada-Iglesias, A. *et al.* A unique chromatin signature uncovers early developmental enhancers in humans. *Nature* **470**, 279–283 (2011).

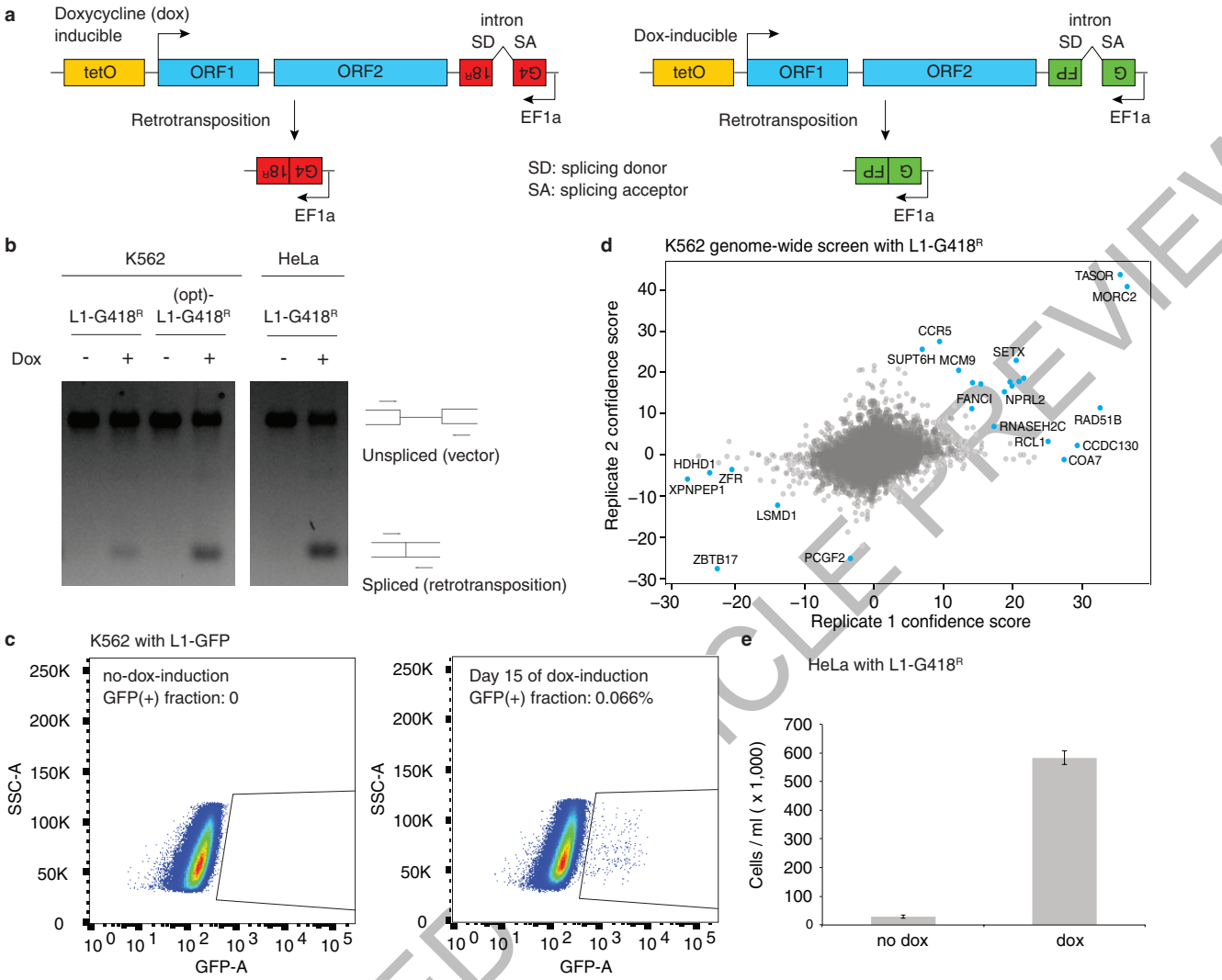

Extended Data Figure 1 | Genome-wide CRISPR/Cas9 screen for L1 regulators in K562 cells. a. Schematic representation of L1-G418^R and L1-GFP reporters used in this work. b. PCR assay on genomic DNA using primers that flank the engineered intron within the G418^R cassette. Two experiments repeated independently with similar results. The spliced PCR bands were not observed prior to dox induction in either K562 or HeLa cells, suggesting that the L1-G418^R reporter was not activated prior to the screening. However, there may exist extremely low level of reporter leakiness that is below the PCR assay detection limits. c. FACS results showing that the L1-GFP cells have no GFP signals without dox-induction (0 out of ~300,000 cells), and begin to produce GFP after dox-induction. Therefore, there is insignificant level of reporter leakiness without dox-induction. Two experiments repeated independently with similar results. d. CasTLE analysis of genome-wide screens in K562 cells, with 20,488 genes represented as individual points. Genes falling under 10% FDR colored in blue, CasTLE likelihood ratio test[11]. n = 2 biologically independent screens. e. HeLa with L1-G418^R are resistant to G418 after dox-induction. 7 days of dox-induction followed by 10 days of G418 selection. Live cells in equal volumes were counted in a single (n = 1) FACS experiment. Center value, total number of live cells. Error bar, square root of total events assuming Poisson distribution of counts.

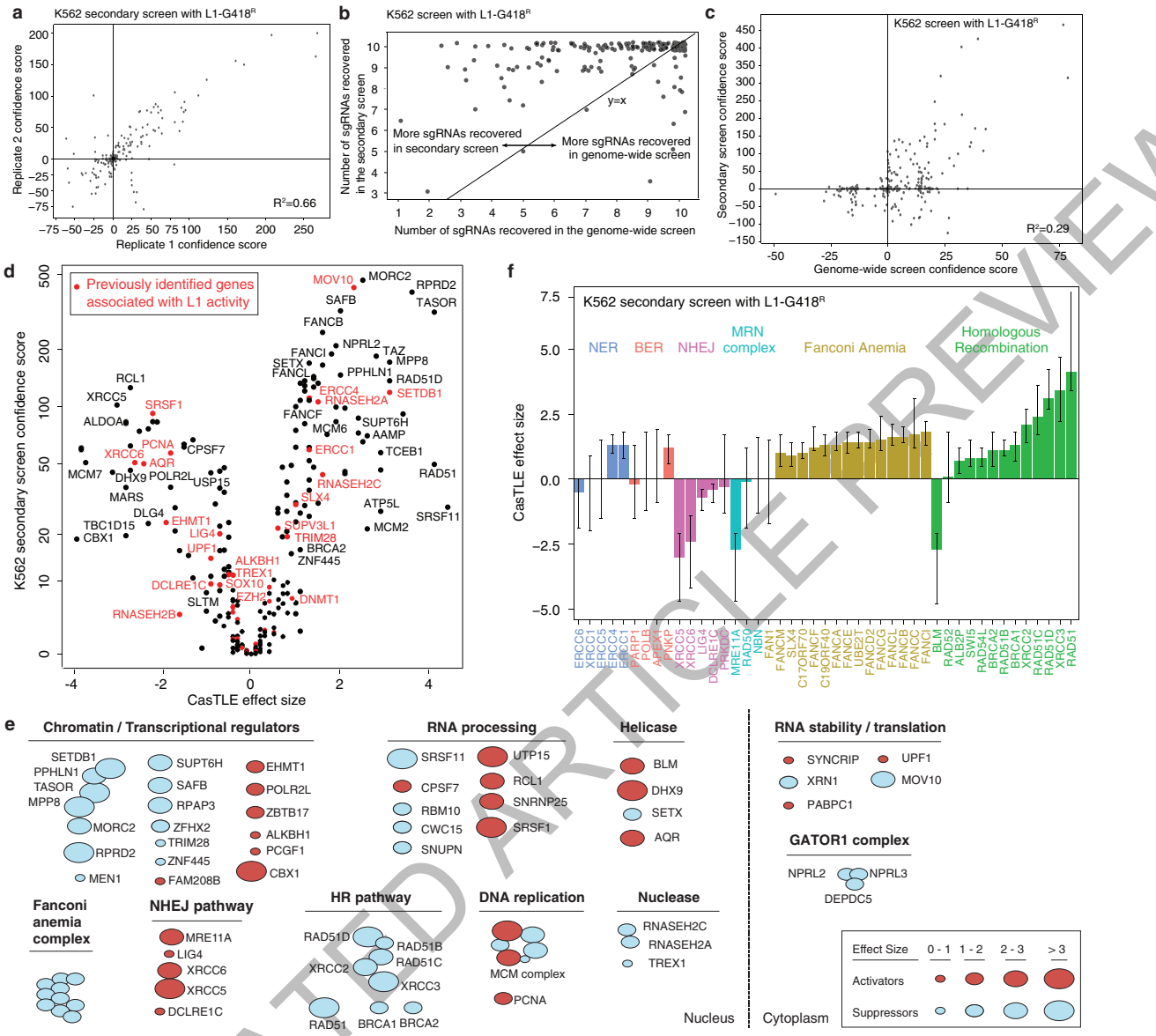

Extended Data Figure 2 | A secondary screen identifies functionally diverse L1 regulators in K562 cells. a. Reproducibility between two independent secondary screens (n = 2) in K562 cells. R-squared value, linear regression model. b. The K562 secondary screen recovers more sgRNAs than the K562 genome-wide screen, suggesting a higher detection sensitivity in the secondary screen. c. Comparison of the secondary screen data (252 genes from n = 2 independent screens) with the genome-wide screen data (n = 2 independent screens) in K562 cells. R-squared value, linear regression model. d. Volcano plot showing K562 secondary screen results (252 genes from two independent screens), with genes previously implicated in L1 biology colored in red. e. Classification diverse L1 activators and suppressors identified in K562 cells by their known biological process. f. The maximum effect size (center value) of indicated DNA repair genes, estimated by CasTLE from two independent K562 secondary screens with 10 different sgRNAs per gene. Error bars, 95% credible intervals of the estimated effect size.

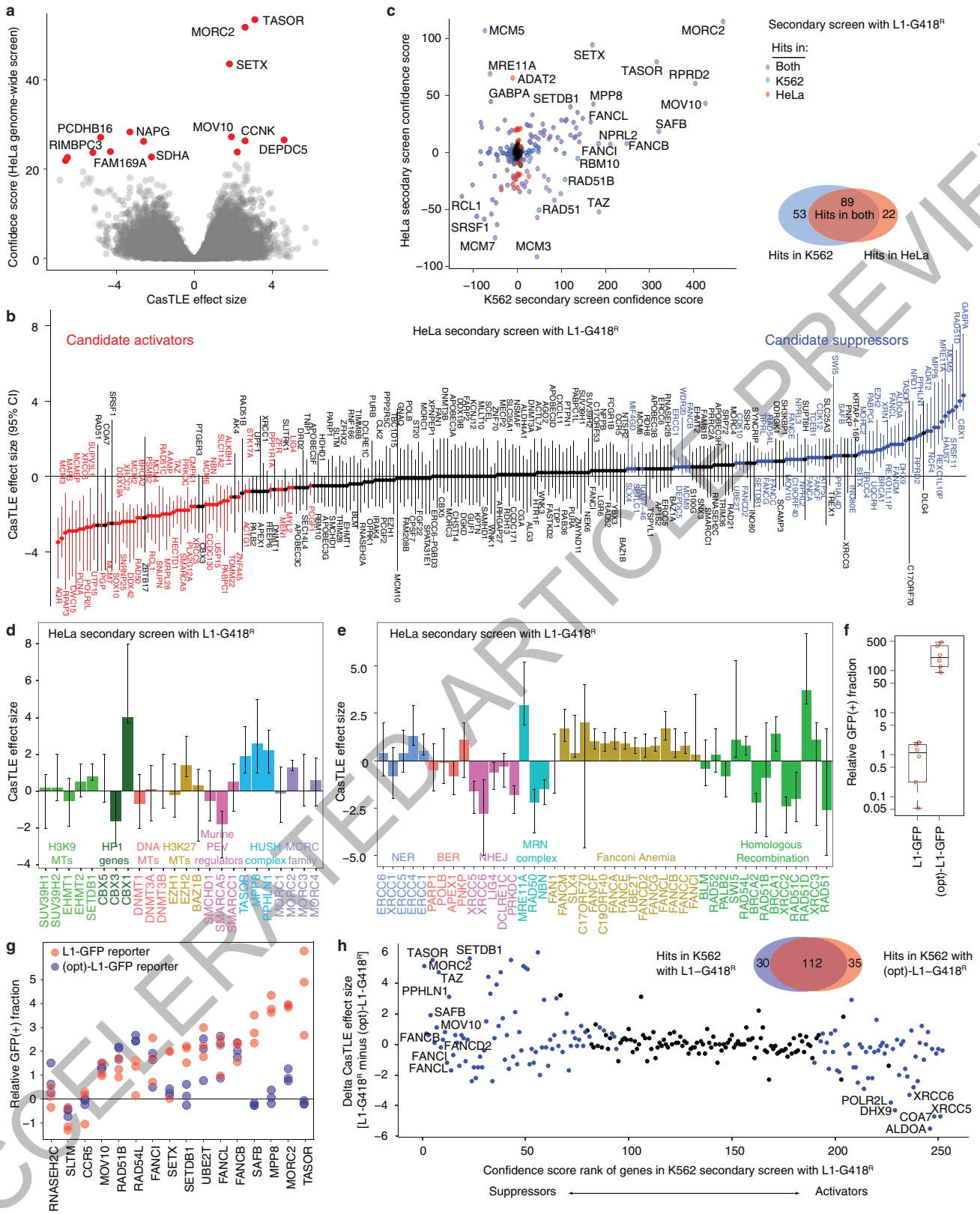

Extended Data Figure 3 | See next page for caption.

Extended Data Figure 3 | Screen for L1 regulators in HeLa cells and and L1- sequence-dependent L1 regulators. a. CasTLE analysis of two independent genome-wide screens in HeLa cells, with 20,514 genes represented as individual points. Genes at 10% FDR cutoff colored in red, CasTLE likelihood ratio test[11]. b. The maximum effect size (center value) estimated by CasTLE from two independent HeLa secondary screens with 10 different sgRNAs per gene. Bars, 95% credible interval (CI). L1 activators, red; L1 suppressors, blue. Genes whose CI include zero are colored in gray and are considered non-effective against L1. c. Scatter plots showing the secondary screen hits identified in K562 cells and HeLa cells (252 genes from two independent screens in each cell line), with Venn diagram comparing hits in the two cell lines is shown on the right. d. The maximum effect size (center value) of indicated heterochromatin regulators, estimated by CasTLE from two independent HeLa secondary screens with 10 different sgRNAs per gene. Error bars, 95% credible intervals of the estimated effect size. e. The maximum effect size (center value) of indicated DNA repair genes, estimated by CasTLE from two independent HeLa secondary screens with 10 different sgRNAs per gene. Error bars, 95% credible intervals of the estimated effect size. f. The (opt)-L1-GFP reporter retrotransposed more frequently than L1-GFP did in K562. The GFP(+) fraction of cells with the indicated L1 reporter after 15 days of dox induction was normalization to the L1-GFP sample. Box plots show median and interquartile range (IQR), whiskers are 1.5× IQR. n = 6 biologically independent replicates. g. The GFP(+) fraction of dox-induced Ctrl and mutant cell pools with the L1-GFP reporter or (opt)-L1-GFP reporter. Experiments were performed as Fig. 1e. Chromatin regulators (e.g. TASOR, MORC2, MPP8, SAFB) did not suppress the (opt)-L1-GFP reporter, in which 24% of the L1 ORF nucleotide sequence is altered, without changes in the encoded amino acid sequence[19,20], indicating their L1 regulation depends on the native nucleotide-sequence of L1Hs. h. K562 secondary screen with the (opt)-L1-G418^R reporter (252 genes from n = 2 independent screens) revealed genes that regulate retrotransposition dependent or nondependent on the native L1 nucleotide sequence. The K562 secondary screen candidates identified with L1-G418^R (252 genes from n = 2 independent screens) were labeled in blue. A Venn diagram comparing hits identified from the two L1-reporters is also shown.

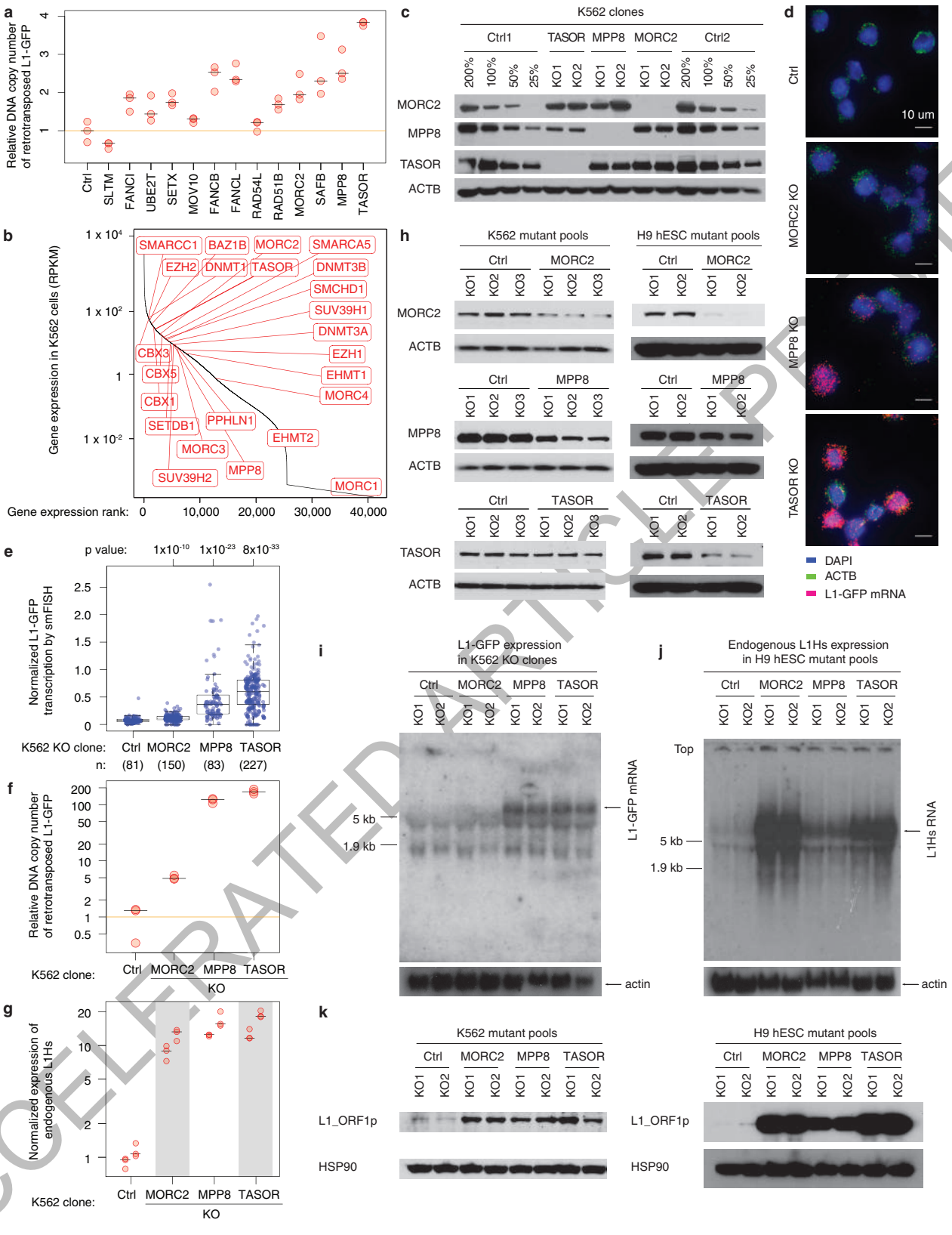

Extended Data Figure 4 | See next page for caption.

Extended Data Figure 4 | MORC2, MPP8 and TASOR silence L1 transcription. a. Relative genomic copy number of newly integrated L1-GFP reporters in the indicated mutant K562 pools after dox-induction. PspGI-assisted qPCR assay used here was designed to selectively detect spliced GFP rather than the unspliced version (see Methods section). The L1-GFP copies were normalized to beta-actin DNAs; data then normalized to Ctrl. As a putative L1 activator, SLTM shows an opposite effect on the DNA copy number, compared with L1 suppressors. Center value as median. n = 3 technical replicates per gene. b. RNA-seq data in Ctrl K562 cells showing that most heterochromatin regulators in Fig. 2a are expressed, supporting the selective effect of HUSH and MORC2 in L1 regulation. c. Western blots validating the knockout (KO) effects in independent KO K562 cell clones. Ctrl samples were loaded at 4 different amounts (200%, 100%, 50%, 25% of KO clones). Three experiments repeated independently with similar results. To obtain KO clones, we sorted mutant K562 pools (cells used in Fig. 1e,f) into 96-well plates, expanded cells and screened for KO clones through western blotting. Of note, all K562 KO clones were derived from the same starting L1-GFP reporter line, and thus do not differ in reporter transgene integrations among the clones. d. Representative images of single molecule FISH (smFISH) assays targeting ACTB mRNAs and RNA transcripts from L1-GFP reporters in Ctrl and KO K562 clones after 5 days of dox-induction. No signal was observed from L1-GFP reporters without dox-induction (data not shown). Two experiments repeated independently with similar results. See also panel e and Fig. 2b (showing L1-GFP mRNA only). e. Quantitation of the L1-GFP transcription level from the indicated number of K562 cells, determined by smFISH assays (panel d and Fig. 2b). The number of L1-GFP mRNA transcripts is normalized to the number of beta-actin mRNAs within each K562 cell. Box plots show median and interquartile range (IQR), whiskers are 1.5× IQR. P-value, two-sided Wilcoxon test. 95% CI for median from 1,000x bootstrap: Control: 0.059-0.082; MORC2: 0.106-0.123; MPP8: 0.264-0.410; TASOR: 0.514-0.671. f. MORC2, MPP8, and TASOR KOs increase the genomic copy number of newly integrated L1-GFP reporters. PspGI-assisted qPCR assays were performed as in panel a), but using clonal KO K562 clones instead of mutant cell pools. Data normalized to Ctrl. n = 3 technical replicates, center value as median. g. MORC2 KO, MPP8 KO, and TASOR KO increase the expression of endogenous L1s. RT-qPCR experiments were performed as in (Fig. 1f), but using clonal KO K562 clones instead of mutant cell pools. n = 2 biological replicates x 3 technical replicates (center value as median). The primers do not target the L1-GFP reporter and the cell lines were not dox-induced, so these RT-qPCR assays will not detect L1-GFP transcripts. h. Western blots showing depletion effects of MORC2, MPP8 and TASOR in the mutant pools of K562 cells (left) and in the mutant pools of H9 hESCs without transgenic L1 reporters (right). Two experiments repeated independently with similar results. i. Northern blots showing increased transcription from the L1-GFP reporter in KO K562 clones (same cell lines as in panel c) after 5 days' dox-induction. Two experiments repeated independently with similar results. As observed in Fig. 2b, while HUSH KO significantly increases L1-GFP transcription, MORC2 KO leads to only a modest increase. This is probably because the L1-GFP reporter does not contain the native L1 5' UTR sequence, where MORC2 intensively binds (See Extended Data Fig. 7f,g). The 5 kb and 1.9 kb marks on the membrane refer to the 28S rRNA and 18S rRNA bands respectively. j. Northern blots showing that disruption of MORC2, MPP8 and TASOR increases the expression level of endogenous L1Hs in hESCs, same cell lines as in panel h). Size marker indicated as in panel i). Two experiments repeated independently with similar results. k. Western blots showing protein abundance of L1_ORF1p and HSP90 in the mutant pools of K562 cells and hESCs (same cell line as shown in panel h). Two experiments repeated independently with similar results. Experiments were performed without dox-induction of the transgenic L1 reporter. Due to the strong signal of bands from the KO samples, the blots were exposed for a very short time and the band signal in the Ctrl samples were relatively very weak compared to the KO samples; same case for panels i, j).

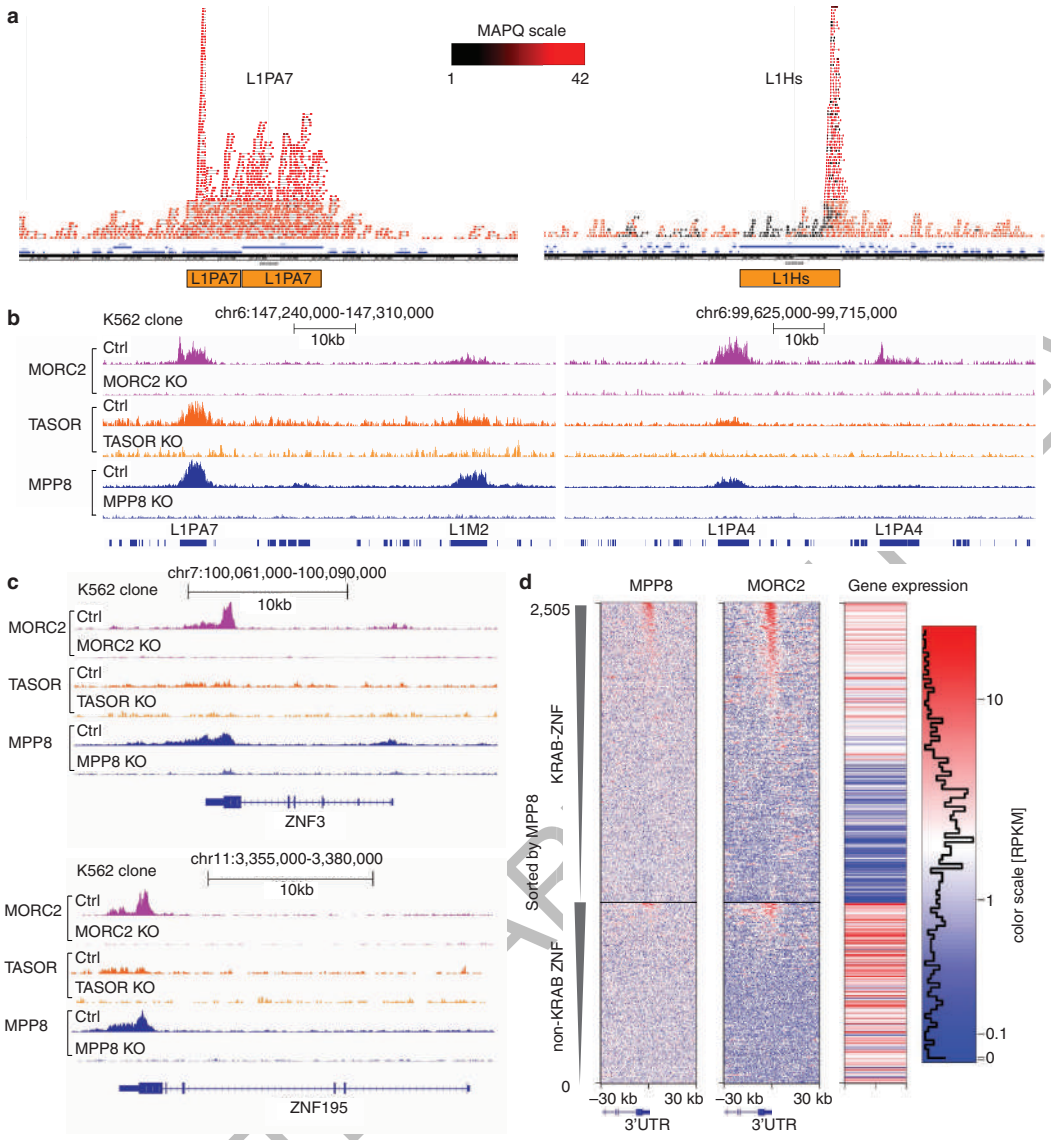

Extended Data Figure 5 | The binding profiles of MORC2, MPP8 and TASOR revealed by ChIP-seq in K562 cells. a. Using a paired-end sequencing strategy for the ChIP-seq, together with the sequence divergence within native L1 elements, we could map ChIP-seq reads to individual L1 instances in the genome. Genome browser snapshots of MORC2 ChIP-seq reads alignment over L1PA7 (left) and L1Hs (right). Experiment was repeated once with similar results. Color scale indicates mapping quality score (MAPQ) for each read pair. MAPQ = 10 log10 p, where p is the probability that true alignment belongs elsewhere. With the exception of L1Hs, which is the youngest and least sequence divergent family, the bodies of L1 repeats are uniquely mappable. In case of L1Hs, the 5'UTR is still mappable to determine the level of L1Hs in Ctrl and KO clones. b. Genome browser snapshots for MPP8 (blue), TASOR (orange) and MORC2 (purple) ChIP-seq read densities from Ctrl and corresponding KO K562 clones at two representative example genomic loci. Experiment was repeated once with similar results. LINE element occurrences are indicated by blue rectangles at the bottom of the plot. Four instances of long L1 elements are named indicating L1 families they belong to. Note complete absence of ChIP-seq signal from KO lines and selectivity toward some but not other L1 instances. Of note, while MPP8 and MORC2 ChIP signals were robust, TASOR ChIPs showed relatively weak enrichments (either due to poor antibody quality or genuine biological properties); for this reason, a subset of our downstream analyses is focused on MORC2 and MPP8. c. In addition to full length L1, HUSH complex and MORC2 bind 3'UTRs of KRAB Zinc Finger (ZNF) genes. Genome browser snapshots of ChIP-seq read densities over representative examples, from both Ctrl and corresponding KO K562 clones. Experiment was repeated once with similar results. d. HUSH complex and MORC2 preferentially bind expressed KRAB-ZNF genes over other ZNF genes. Heatmaps of MPP8 (left) and MORC2 (center) signals over 2,600 ZNF genes, centered in the 3' end of the genes and sorted first by the presence of KRAB domain and then by MPP8 ChIP signal. Upper 1,600 genes are KRAB-ZNF, lower 1,000 non-KRAB ZNF genes. Right heatmaps codes absolute expression level of each gene in RPKM scale from the K562 RNA-seq data (rightmost panel).

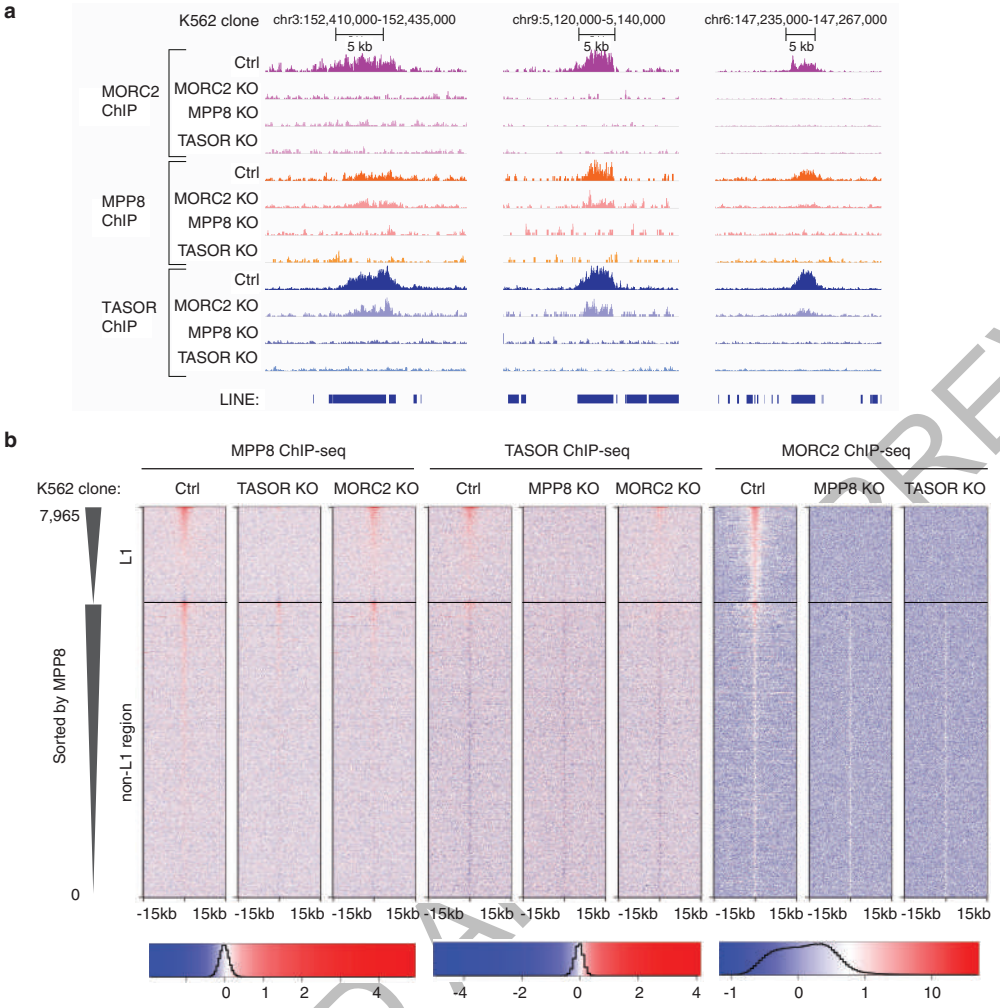

Extended Data Figure 6 | HUSH and MORC2 collaborate at binding target L1s. a. Representative genome browser view of normalized ChIP-seq read densities over L1 elements. Experiment was repeated once with similar results. Loss of MPP8 and TASOR results in no detectable binding by MORC2, MPP8 and TASOR, while loss of MORC2 results in partially diminished recruitment of HUSH complex subunits. b. Heatmaps of MPP8 (left), TASOR (center) and MORC2 (right) ChIP-seq signals subtracted for ChIP signal from corresponding KO lines. Heatmaps are centered on MPP8 and MORC2 peaks, separated by the presence or absence of underlying L1 and then sorted by MPP8 ChIP signal strength. Loss of MORC2 has only partial effect on recruitment of MPP8 and TASOR to the L1 elements, while loss of either MPP8 or TASOR abrogates MORC2 recruitment.

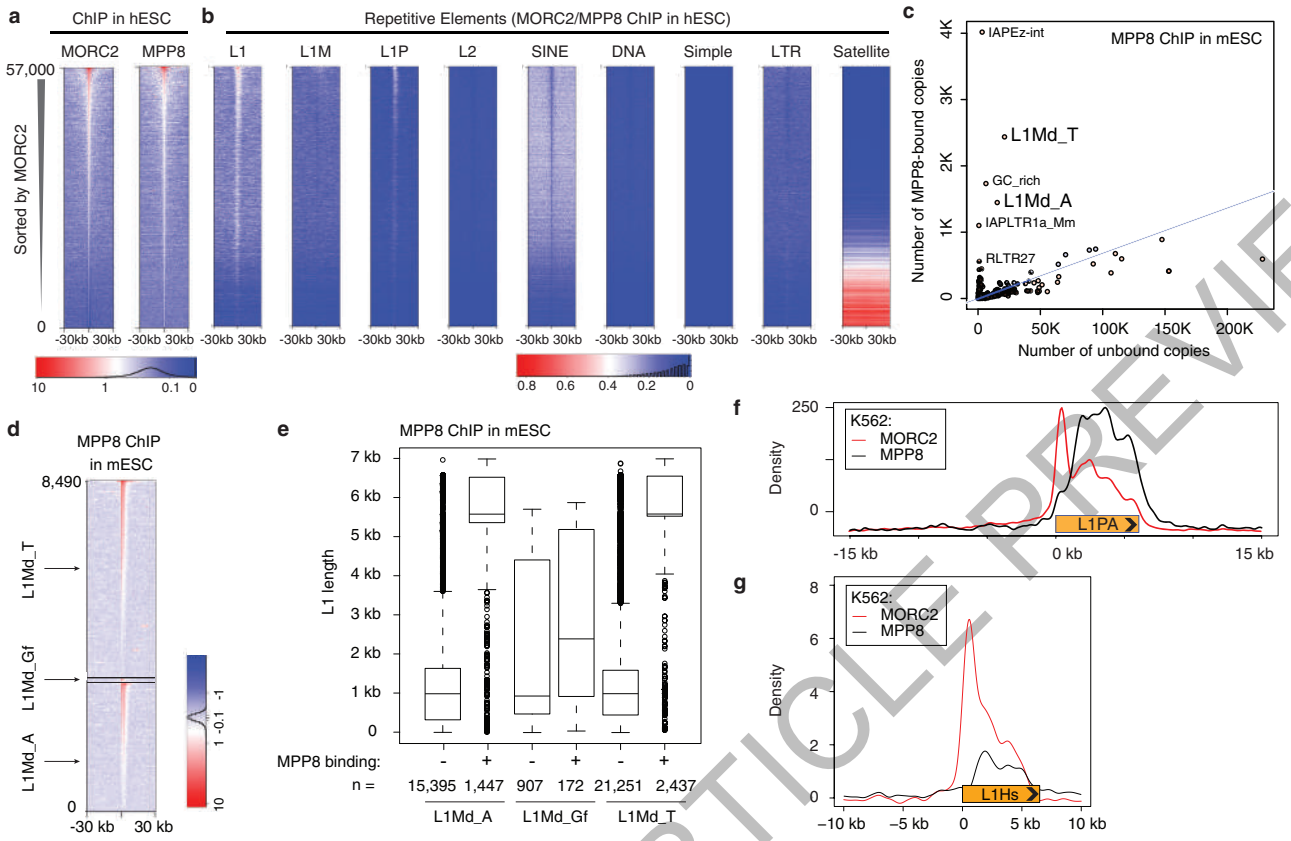

Extended Data Figure 7 | HUSH/MORC2 preferentially bind full-length L1 instances in human ESCs, mouse ESCs and K562 cells. a. Widespread genomic co-binding of MPP8 and MORC2 in hESCs. Heatmap representation of ChIP-seq results at 57,000 genomic loci, centered on MPP8 and MORC2 summits and sorted by MORC2 ChIP-seq signal. Plotted is normalized ChIP read density from hESCs. b. Heatmaps of MORC2/MPP8 ChIP-seq density over indicated repeat classes, centered and sorted as in panel a. HUSH complex and MORC2 bind predominantly to L1 elements in hESCs, in particular to the primate-specific L1P families, suggesting that HUSH/MORC2-dependent silencing is relevant in many embryonic and somatic cell types. c. L1 families that encompass active L1 copies, such as L1Md-T and L1Md-A, are significantly enriched among MPP8 binding sites in mouse ESC. L1Md_Gf is also enriched but not shown due to the low number of instances. Thus, HUSH-mediated L1 regulation appears to be conserved among species. Of note, MPP8 is also strongly enriched at IAP elements, a class of murine endogenous retroviruses that remain currently mobile in the mouse genome. d. MPP8 ChIP-seq heatmaps in mESCs featuring retrotransposition-competent L1Md-T, L1Md-A and L1Md-Gf. e. MPP8 preferentially bind full-length L1Md-A and L1Md-T in mESCs. Plotted is size distribution of the indicated L1 instances that overlap with MPP8 ChIP-seq peaks, or remaining L1s that do not overlap with such ChIP-seq signals. Box plots show median and interquartile range (IQR), whiskers are 1.5× IQR. f. Aggregate plots of MORC2 (red) and MPP8 (black) ChIP-seq signals over 500 full-length, MPP8-bound L1PAs, centered on the L1 5' end. g. Aggregate plots of MORC2 (red) and MPP8 (black) ChIP-seq signals on L1Hs (L1PA1). Similar as the binding profile on L1PA (panel f), MPP8/MORC2 occupy the whole body of L1Hs, with MORC2 additionally binding L1Hs 5'UTR. Please note that ChIP-seq fragments are much less likely to be uniquely mapped, and thus removed by the alignment criteria, within the L1Hs non-5'UTR region, due to their minimal sequence divergence (Extended Data Fig. 5a).

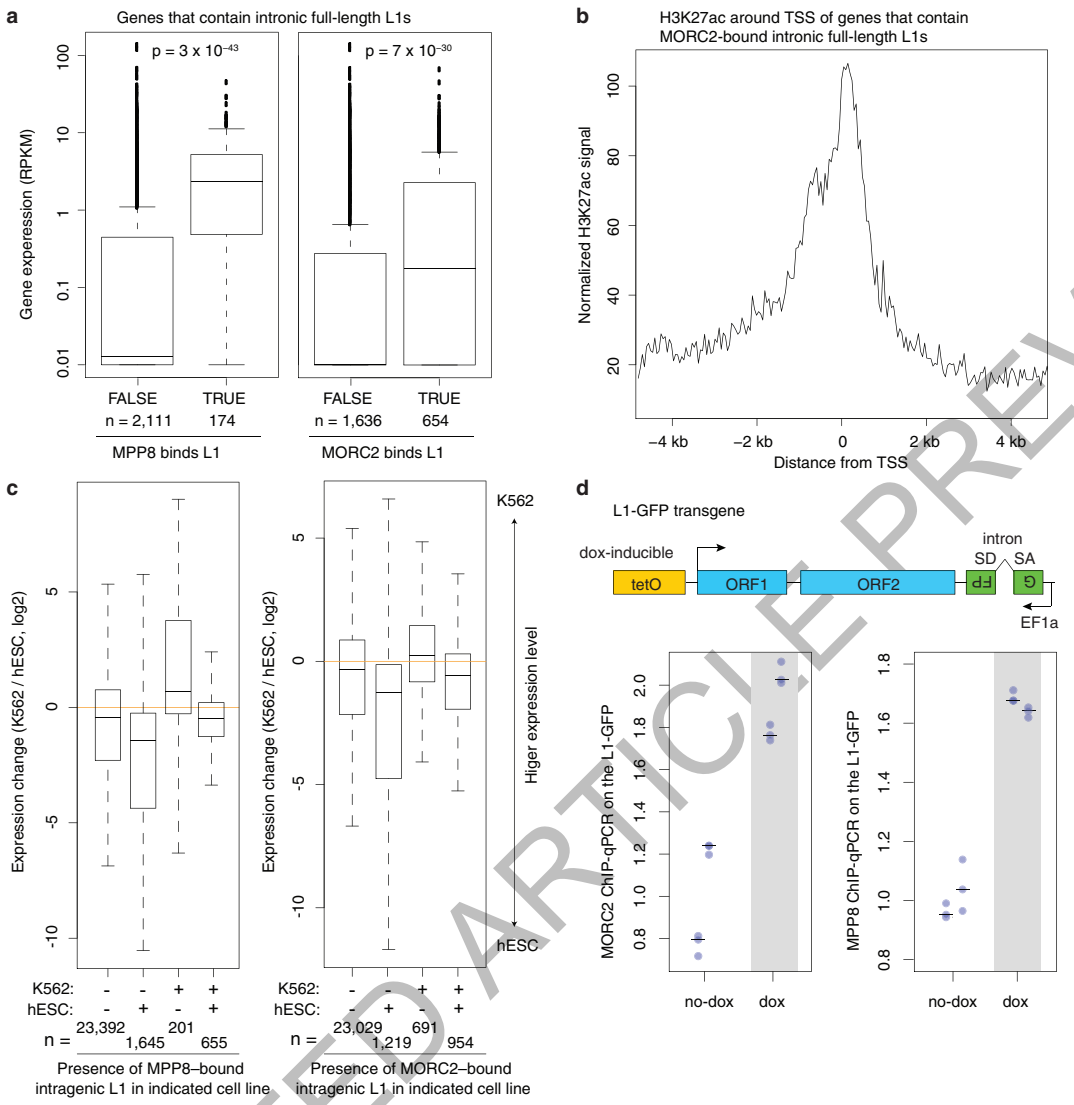

Extended Data Figure 8 | HUSH/MORC2 preferentially bind intronic L1s within actively transcribed genes. a. Genes that contain MPP8 or MORC2 bound intronic L1s are expressed at significantly higher levels in Ctrl K562 cells, compared to genes that contain intronic full-length L1s unbound by MPP8 or MORC2. p-value, two-sided Mann-Whitney-Wilcoxon test. Box plots show median and interquartile range (IQR), whiskers are 1.5× IQR. b. The promoters of genes that contain MPP8 or MORC2 bound intronic full-length L1s are marked by transcriptionally permissive H3K27ac in wild-type K562 cells. H3K27ac ChIP-seq data are taken from K562 epigenome pilot study, accession number PRJEB8620. TSS, transcription start site. c. Genes selectively occupied by MORC2/MPP8 either in K562 or in hESC cells exhibit higher gene expression in the corresponding cell line (p-values = 4.3×10^{-107} for MPP8 binding; p-values = 5.0×10^{-92} for MORC2 binding, Kruskal-Wallis test). Boxplots defined as in panel a. RNA-seq datasets for hESC are from SRA entries SRR2043329 and SRR2043330. d. ChIP-qPCR assays quantifying HUSH/MORC2 binding to an inducible L1 transgene in K562 cells before or after its transcriptional induction via Dox. Transcriptional induction increases binding of MORC2 and MPP8 to the L1 transgene. n = 2 biological replicates x 3 technical replicates (center value as median).

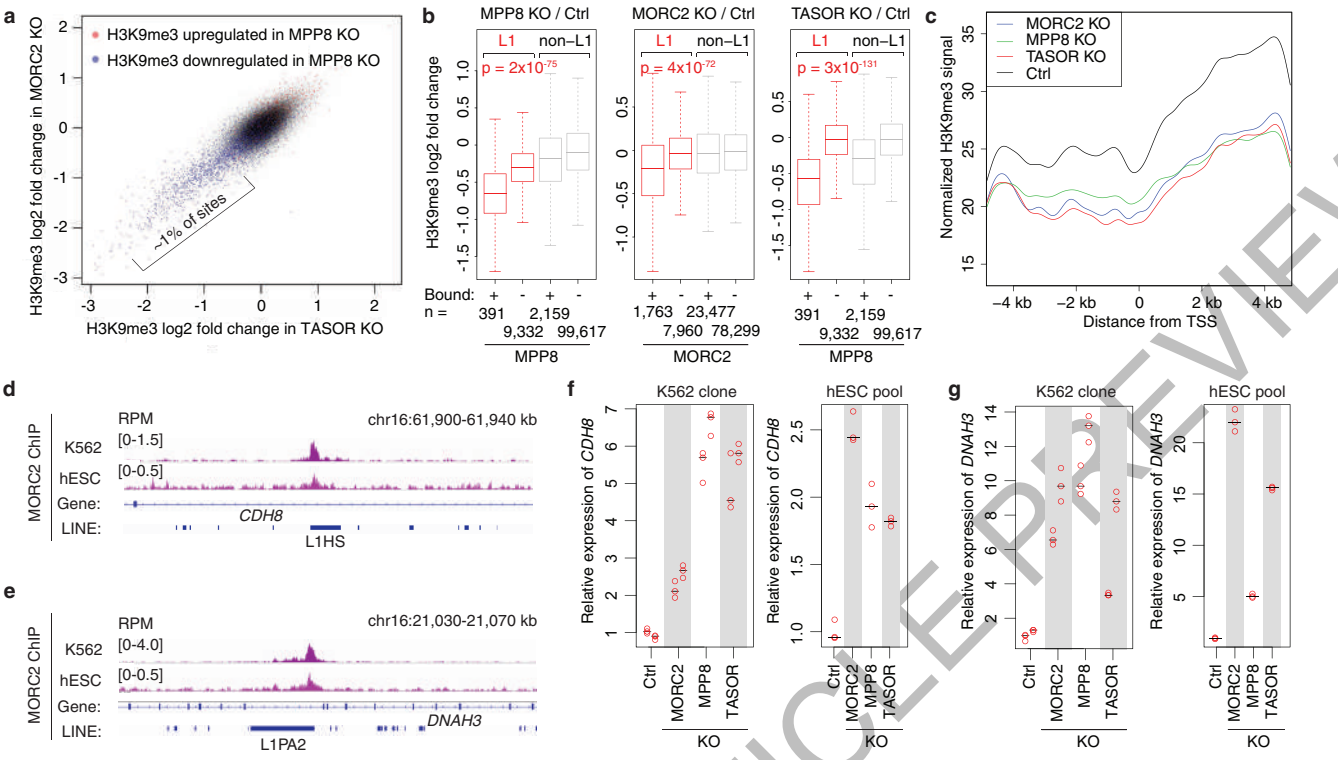

Extended Data Figure 9 | HUSH/MORC2 facilitate H3K9me3 at their L1 targets for transcription repression. a. Concordant subset (~1%) of (n = 111,499) H3K9me3 sites in the genome lose H3K9me3 signal in MORC2 KO, MPP8 KO and TASOR KO K562 clones. Two independent lines each for WT, MORC2KO, TASOR KO, MPP8 KO. Plotted is log2 fold change in H3K9me3 ChIP signal in TASOR KO relative to Ctrl (x-axis) and log2 fold change in H3K9me3 ChIP signal in MORC2 KO relative to Ctrl (y-axis). Points are color coded with blue sites having significant H3K9me3 loss in MPP8 KO, red sites significantly gaining the signal in MPP8 KO, while gray have no detectable change. Sites that significantly lose H3K9me3 signal in KO line are more likely to have corresponding loss in other KO lines. Odds ratios: 26.23 with 95% confidence intervals (CI) [23,66, 29.10] for MORC2 versus MPP8; 21.70 with 95% CI [19.75, 23.83] for TASOR versus MPP8; 122.53 with 95% CI [109.21, 137.43] for TASOR versus MORC2. P = 0 each case, two-sided Fisher's exact test. b. Genomic sites that exhibit the strongest loss of H3K9me3 in MORC2, MPP8 or TASOR KOs are preferentially L1 occupied by these factors. Boxplots of log2 fold change in H3K9me3 relative to Ctrl for MPP8 KO (left), MORC2 KO (center) and TASOR KO (right). Box plots show median and interquartile range (IQR), whiskers are 1.5 × IQR. MPP8 and MORC2 bound L1s show significant loss of H3K9me3 (p-values, two-sided Mann-Whitney-Wilcoxon test). c. Averaged distribution of H3K9me3 ChIP-seq signals in Ctrl and KO K562 clones over the host genes that contain the MORC2-targeted intronic full-length L1s, centered on the transcription start site (TSS) of the host genes. d. Genome browser showing MORC2 binding at the intronic full-length L1Hs within *CDH8* in both K562 and hESCs. Experiment was repeated once with similar results. e. Genome browser showing MORC2 binding at the intronic full-length L1PA2 within *DNAH3* in both K562 and hESCs. Experiment was repeated once with similar results. f. Depletion of MORC2/HUSH increases the expression of *CDH8* in both K562 (n = 2 biological replicates x 3 technical replicates) and hESCs (n = 3 technical replicates), as measured by RT-qPCR assay. The *CDH8* expression level was normalized to beta-actin mRNA. All samples were then normalized to Ctrl sample. Center value as median. g. Depletion of MORC2/HUSH increases the expression of *DNAH3* in both K562 (n = 2 biological replicates x 3 technical replicates) and hESCs (n = 3 technical replicates), as measured by RT-qPCR assay. The *DNAH3* expression level was normalized to beta-actin mRNA. All samples were then normalized to Ctrl sample. Center value as median.

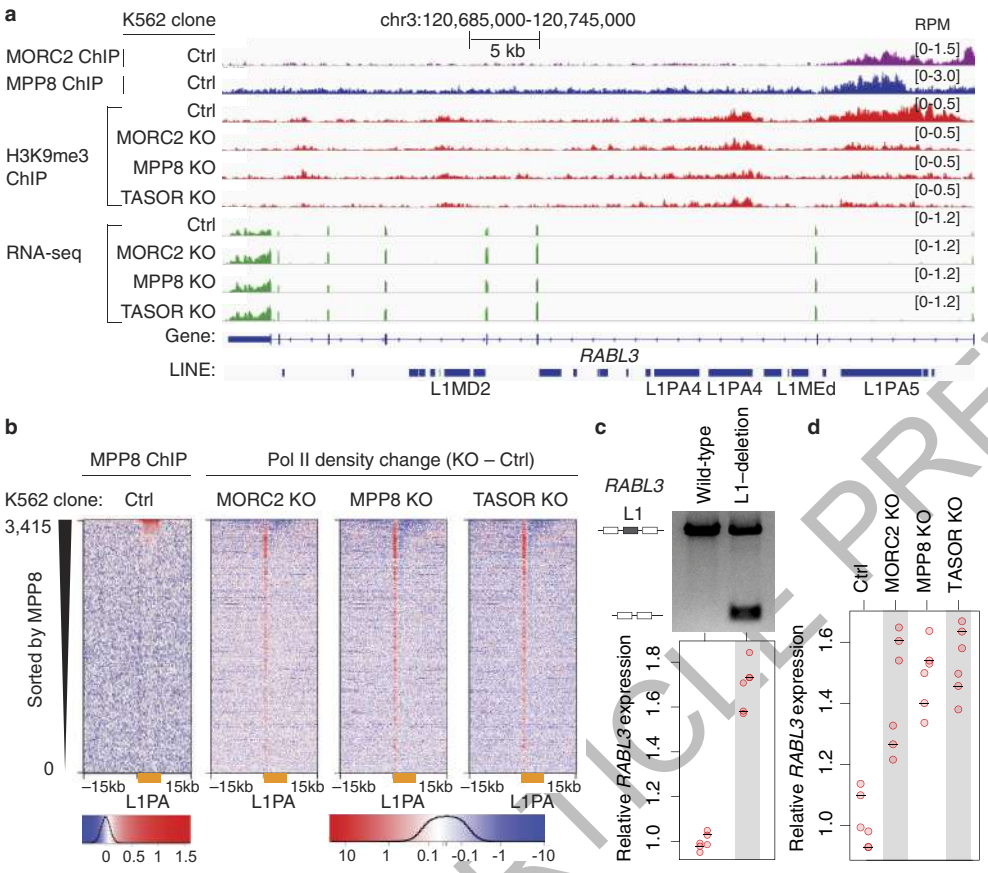

Extended Data Figure 10 | HUSH/MORC2 binding at intronic L1s results in the decreased expression of active host genes. a. Genome browser tracks illustrating loss of HUSH/MORC2 causing decreased H3K9me3 over the intronic L1PA5 element and concomitant increase in the expression of host gene *RABL3*. Experiment was repeated once with similar results. b. Loss of HUSH/MORC2 leads to increased Pol II signals at 5'UTR and decreased Pol II signals within L1 bodies at HUSH-bound L1PA elements (orange bars). Heatmaps show Pol II density change in KO K562 clones compared to Ctrl, centered on the L1 5' end and sorted by MPP8 ChIP signal. c. Deletion of the intronic L1 within *RABL3* causes increased *RABL3* expression. Upper panel: an agarose gel analysis of the PCR assay with primers flanking the HUSH/MORC2-bound intronic L1; two experiments repeated independently with similar results. Lower panel: RT-qPCR analysis of *RABL3* expression. The *RABL3* expression level was normalized to beta-actin mRNA. All samples were then normalized to wild-type sample. n = 2 biological replicates x 3 technical replicates (center value as median). d. Depletion of MORC2, MPP8, TASOR increases *RABL3* expression. RT-qPCR data normalized as in panel c). n = 2 biological replicates x 3 technical replicates (center value as median).

nature research

Corresponding author(s): Joanna Wysocka and Michael Bassik

☐ Initial submission ☐ Revised version ☒ Final submission

Life Sciences Reporting Summary

Nature Research wishes to improve the reproducibility of the work that we publish. This form is intended for publication with all accepted life science papers and provides structure for consistency and transparency in reporting. Every life science submission will use this form; some list items might not apply to an individual manuscript, but all fields must be completed for clarity.

For further information on the points included in this form, see Reporting Life Sciences Research. For further information on Nature Research policies, including our data availability policy, see Authors & Referees and the Editorial Policy Checklist.

Experimental design

1. Sample size

Describe how sample size was determined.

For the screen, two independent replicate screens were performed, which are sufficient for screening technologies. See Methods section, 'Genome-wide screen in K562 cells', 'Secondary screen in K562 cells' and 'Genome-wide screen and secondary screen in HeLa cells'.

2. Data exclusions

Describe any data exclusions.

No data was excluded.

3. Replication

Describe whether the experimental findings were reliably reproduced.

Once experiments and procedures were fully optimized, all attempts at replication were successful.

4. Randomization

Describe how samples/organisms/participants were allocated into experimental groups.

K562 KO clones were allocated into experimental groups based on their genotype (Extended Data Figure 4c). For smFISH experiments, individual cells were allocated into experimental groups based on their genotype (Figure 2b and Extended Data Figure 4d).

5. Blinding

Describe whether the investigators were blinded to group allocation during data collection and/or analysis.

Blinding was performed during the smFISH data analyses (Extended Data Figure 4e), where B.G. who analyzed smFISH images was blinded to all conditions.

Note: all studies involving animals and/or human research participants must disclose whether blinding and randomization were used.

6. Statistical parameters

For all figures and tables that use statistical methods, confirm that the following items are present in relevant figure legends (or in the Methods section if additional space is needed).

n/a	Confirmed
☐	☒ The exact sample size (*n*) for each experimental group/condition, given as a discrete number and unit of measurement (animals, litters, cultures, etc.)
☐	☒ A description of how samples were collected, noting whether measurements were taken from distinct samples or whether the same sample was measured repeatedly
☐	☒ A statement indicating how many times each experiment was replicated
☐	☒ The statistical test(s) used and whether they are one- or two-sided (note: only common tests should be described solely by name; more complex techniques should be described in the Methods section)
☐	☒ A description of any assumptions or corrections, such as an adjustment for multiple comparisons
☐	☒ The test results (e.g. *P* values) given as exact values whenever possible and with confidence intervals noted
☐	☒ A clear description of statistics including central tendency (e.g. median, mean) and variation (e.g. standard deviation, interquartile range)
☐	☒ Clearly defined error bars

See the web collection on statistics for biologists for further resources and guidance.

Software

Policy information about availability of computer code

7. Software

Describe the software used to analyze the data in this study.	For Images analyses we used MATLAB 2016b (MathWorks). Flowjo 9.9 was used for flow cytometry analyses. For statistical analysis we used R 3.3.2. For ChIP-seq genomic alignments we used bowtie2 v.2.2.9, peak calls with MACS2 v2.1.1.20160309, IGV_2.3.92 and IGB 9.0.0 for visualization, bedtools v2.17.0 and GNU awk 4.1.3 for overlap statistics and genome interval manipulation. For humans hg38 reference genome was used, for mouse mm10. RNAseq alignments were performed with hisat2 v2..0.5, followed by stringtie v 1.3.3b and featureCounts v1.4.6-p2, further analysis was performed with Bioconductor 3.4 and DESeq2 1.14.1, human genocde 25 transcript models were used.

For manuscripts utilizing custom algorithms or software that are central to the paper but not yet described in the published literature, software must be made available to editors and reviewers upon request. We strongly encourage code deposition in a community repository (e.g. GitHub). *Nature Methods* guidance for providing algorithms and software for publication provides further information on this topic.

Materials and reagents

Policy information about availability of materials

8. Materials availability

Indicate whether there are restrictions on availability of unique materials or if these materials are only available for distribution by a for-profit company.	No restrictions.

9. Antibodies

Describe the antibodies used and how they were validated for use in the system under study (i.e. assay and species).	1) Rabbit MORC2 antibody (A300-149A, Bethyl Laboratories), validated by vendor, and used in previous literature. 2) Rabbit MPP8 antibody (16796-1-AP, Protein Technologies Inc), validated by vendor, and used in previous literature. 3) Rabbit TASOR antibody (HPA006735, Atlas Antibodies), validated by vendor, and used in previous literature. 3) Mouse anti-LINE-1 ORF1p antibody (MABC1152, Millipore), validated by vendor, and used in previous literature. 4) Rabbit HSP90 (C45G5, Cell Signalling, #4877), Extensively used in the literature. 5) Beta actin antibody (ab49900, Abcam), Extensively used in the literature. 6) Histone H3 (tri-methyl K9) antibody (ab8898, Abcam), validated by vendor, and used in previous literature. 7) RNA Pol II (Santa Cruz Biotechnology, N-20 sc-899), validated by vendor, and used in previous literature.

10. Eukaryotic cell lines

a. State the source of each eukaryotic cell line used.	Cell lines are from commercial sources. HeLa and K562: ATCC Human Embryonic Stem Cells, H9: WiCell Mouse Embryonic Stem Cells, ES-E14TG2a: ATCC
b. Describe the method of cell line authentication used.	Cell lines were authenticated by the vendor. All cells were obtained from comerical sources. HeLa, K562 and mESC (ATCC). Human Embryonic Stem Cells H9 (WiCell).
c. Report whether the cell lines were tested for mycoplasma contamination.	Cell cultures were routinely tested and found negative for mycoplasma infection (MycoAlert, Lonza).
d. If any of the cell lines used are listed in the database of commonly misidentified cell lines maintained by ICLAC, provide a scientific rationale for their use.	None of the cell lines used in this study are in the database of commonly misidentified cell lines.

Animals and human research participants

Policy information about studies involving animals; when reporting animal research, follow the ARRIVE guidelines

11. Description of research animals

Provide details on animals and/or animal-derived materials used in the study.	No animals were used in this study.

Policy information about studies involving human research participants

12. Description of human research participants

Describe the covariate-relevant population characteristics of the human research participants.	This study did not involve human research participants.

nature research

Corresponding author(s): Joanna Wysocka, Michael Bassik

☐ Initial submission ☐ Revised version ☒ Final submission

ChIP-seq Reporting Summary

Form fields will expand as needed. Please do not leave fields blank.

Data deposition

1. For all ChIP-seq data:

☒ a. Confirm that both raw and final processed data have been deposited in a public database such as GEO.

☒ b. Confirm that you have deposited or provided access to graph files (e.g. BED files) for the called peaks.

2. Provide all necessary reviewer access links.
The entry may remain private before publication.

https://www.ncbi.nlm.nih.gov/geo/query/acc.cgi?token=ojerwuukpzsbjsb&acc=GSE95374

3. Provide a list of all files available in the database submission.

GSM2509455
ChIP:MORC2_Cell:WT_rep1
GSM2509456
ChIP:MORC2_Cell:WT_rep2
GSM2509457
ChIP:MORC2_Cell:MORC2-KO_rep1
GSM2509458
ChIP:MORC2_Cell:MORC2-KO_rep2
GSM2509459
ChIP:MORC2_Cell:MPP8-KO_rep1
GSM2509460
ChIP:MORC2_Cell:MPP8-KO_rep2
GSM2509461
ChIP:MORC2_Cell:TASOR-KO_rep1
GSM2509462
ChIP:MORC2_Cell:TASOR-KO_rep2
GSM2509463
ChIP:MPP8_Cell:WT_rep1
GSM2509464
ChIP:MPP8_Cell:WT_rep2
GSM2509465
ChIP:MPP8_Cell:MORC2-KO_rep1
GSM2509466
ChIP:MPP8_Cell:MORC2-KO_rep2
GSM2509467
ChIP:MPP8_Cell:MPP8-KO_rep1
GSM2509468
ChIP:MPP8_Cell:MPP8-KO_rep2
GSM2509469
ChIP:MPP8_Cell:TASOR-KO_rep1
GSM2509470
ChIP:MPP8_Cell:TASOR-KO_rep2
GSM2509471
ChIP:TASOR_Cell:WT_rep1
GSM2509472
ChIP:TASOR_Cell:WT_rep2
GSM2509473
ChIP:TASOR_Cell:MORC2-KO_rep1
GSM2509474
ChIP:TASOR_Cell:MORC2-KO_rep2

GSM2509475
ChIP:TASOR_Cell:MPP8-KO_rep1
GSM2509476
ChIP:TASOR_Cell:MPP8-KO_rep2
GSM2509477
ChIP:TASOR_Cell:TASOR-KO_rep1
GSM2509478
ChIP:TASOR_Cell:TASOR-KO_rep2
GSM2509479
ChIP:Input(MORC2, MPP8, TASOR)_Cell:WT_rep1
GSM2509480
ChIP:Input(MORC2, MPP8, TASOR)_Cell:WT_rep2
GSM2509481
ChIP:Input(MORC2, MPP8, TASOR)_Cell:MORC2-KO_rep1
GSM2509482
ChIP:Input(MORC2, MPP8, TASOR)_Cell:MORC2-KO_rep2
GSM2509483
ChIP:Input(MORC2, MPP8, TASOR)_Cell:MPP8-KO_rep1
GSM2509484
ChIP:Input(MORC2, MPP8, TASOR)_Cell:MPP8-KO_rep2
GSM2509485
ChIP:Input(MORC2, MPP8, TASOR)_Cell:TASOR-KO_rep1
GSM2509486
ChIP:Input(MORC2, MPP8, TASOR)_Cell:TASOR-KO_rep2
GSM2509487
ChIP:H3K9me3_Cell:WT_rep1
GSM2509488
ChIP:H3K9me3_Cell:WT_rep2
GSM2509489
ChIP:H3K9me3_Cell:MORC2-KO_rep1
GSM2509490
ChIP:H3K9me3_Cell:MORC2-KO_rep2
GSM2509491
ChIP:H3K9me3_Cell:TASOR-KO_rep1
GSM2509492
ChIP:H3K9me3_Cell:TASOR-KO_rep2
GSM2509493
ChIP:Input(H3K9me3)_Cell:WT_rep1
GSM2509494
ChIP:Input(H3K9me3)_Cell:WT_rep2
GSM2509495
ChIP:Input(H3K9me3)_Cell:MORC2-KO_rep1
GSM2509496
ChIP:Input(H3K9me3)_Cell:MORC2-KO_rep2
GSM2509497
ChIP:Input(H3K9me3)_Cell:TASOR-KO_rep1
GSM2509498
ChIP:Input(H3K9me3)_Cell:TASOR-KO_rep2
GSM2509503
ChIP:H3K9me3_Cell:WT_rep3
GSM2509504
ChIP:H3K9me3_Cell:WT_rep4
GSM2509505
ChIP:H3K9me3_Cell:MPP8-KO_rep1
GSM2509506
ChIP:H3K9me3_Cell:MPP8-KO_rep2
GSM2509507
ChIP:Input(H3K9me3)_Cell:WT_rep1
GSM2509508
ChIP:Input(H3K9me3)_Cell:WT_rep2

GSM2509509
ChIP:Input(H3K9me3)_Cell:MPP8-KO_rep1
GSM2509510
ChIP:Input(H3K9me3)_Cell:MPP8-KO_rep2
GSM2789802
ChIP:PolII_Cell_K562:WT_rep1
GSM2789803
ChIP:PolII_Cell_K562:WT_rep2
GSM2789804
ChIP:PolII_Cell_K562:MORC2-KO_rep1
GSM2789805
ChIP:PolII_Cell_K562:MORC2-KO_rep2
GSM2789806
ChIP:PolII_Cell_K562:MPP8-KO_rep1
GSM2789807
ChIP:PolII_Cell_K562:MPP8-KO_rep2
GSM2789808
ChIP:PolII_Cell_K562:TASOR-KO_rep1
GSM2789809
ChIP:PolII_Cell_K562:TASOR-KO_rep2
GSM2789810
ChIP:Input_Cell_K562:WT_rep1
GSM2789811
ChIP:Input_Cell_K562:WT_rep2
GSM2789812
ChIP:MPP8_Cell_hESC:WT_rep1
GSM2789813
ChIP:MPP8_Cell_hESC:WT_rep2
GSM2789814
ChIP:MORC2_Cell_hESC:WT_rep1
GSM2789815
ChIP:MORC2_Cell_hESC:WT_rep2
GSM2789816
ChIP:Input_Cell_hESC:WT_rep1
GSM2789817
ChIP:Input_Cell_hESC:WT_rep2
GSM2789818
ChIP:MPP8_Cell_mESC:WT_rep1
GSM2789819
ChIP:MPP8_Cell_mESC:WT_rep2
GSM2789820
ChIP:Input_Cell_mESC:WT_rep1
GSM2789821
ChIP:Input_Cell_mESC:WT_rep2
MORC2KO1_CHIP_INPUT_1.bw
MORC2KO1_CHIP_INPUT.bw
MORC2KO1_CHIP_K9me3.bw
MORC2KO1_CHIP_MORC2_1.bw
MORC2KO1_CHIP_MPP8_1.bw
MORC2KO1_CHIP_TASOR_1.bw
MORC2KO2_CHIP_INPUT_1.bw
MORC2KO2_CHIP_INPUT.bw
MORC2KO2_CHIP_K9me3.bw
MORC2KO2_CHIP_MORC2_1.bw
MORC2KO2_CHIP_MPP8_1.bw
MORC2KO2_CHIP_TASOR_1.bw
MPP8_1.bw
MPP8_2.bw
MPP8KO1_CHIP_INPUT_1.bw
MPP8KO1_CHIP_INPUT_K9_1.bw

MPP8KO1_CHIP_K9me3.bw
MPP8KO1_CHIP_MORC2_1.bw
MPP8KO1_CHIP_MPP8_1.bw
MPP8KO1_CHIP_TASOR_1.bw
MPP8KO2_CHIP_INPUT_1.bw
MPP8KO2_CHIP_INPUT_K9.bw
MPP8KO2_CHIP_K9me3.bw
MPP8KO2_CHIP_MORC2_1.bw
MPP8KO2_CHIP_MPP8_1.bw
MPP8KO2_CHIP_TASOR_1.bw
SAFE_1.bw
SAFE_2.bw
TASOR_1.bw
TASOR_2.bw
TASORKO1_CHIP_INPUT_1.bw
TASORKO1_CHIP_INPUT.bw
TASORKO1_CHIP_K9me3.bw
TASORKO1_CHIP_MORC2_1.bw
TASORKO1_CHIP_MPP8_1.bw
TASORKO1_CHIP_TASOR_1.bw
TASORKO2_CHIP_INPUT_1.bw
TASORKO2_CHIP_INPUT.bw
TASORKO2_CHIP_K9me3.bw
TASORKO2_CHIP_MORC2_1.bw
TASORKO2_CHIP_MPP8_1.bw
TASORKO2_CHIP_TASOR_1.bw
WT1_CHIP_INPUT_1.bw
WT1_CHIP_INPUT.bw
WT1_CHIP_INPUT_K9.bw
WT1_CHIP_K9me3.bw
WT1_CHIP_MORC2_1.bw
WT1_CHIP_MPP8_1.bw
WT1_CHIP_TASOR_1.bw
WT2_CHIP_INPUT_1.bw
WT2_CHIP_INPUT.bw
WT2_CHIP_INPUT_K9.bw
WT2_CHIP_K9me3.bw
WT2_CHIP_MORC2_1.bw
WT2_CHIP_MPP8_1.bw
WT2_CHIP_TASOR_1.bw
hESC_Input1.bw
hESC_Input2.bw
hESC_MORC2_ChIP1.BW
hESC_MORC2_ChIP2.BW
hESC_MPP8_ChIP1.BW
hESC_MPP8_ChIP2.BW
INPUT_1.bw
INPUT_2.bw
INPUT_mESC1.bw
INPUT_mESC2.bw
MPP8_mESC1.bw
MPP8_mESC2.bw
PolII_MORC2_KO1.bw
PolII_MORC2_KO2.bw
PolII_MPP8_KO1.bw
PolII_MPP8_KO2.bw
PolII_TASOR_KO1.bw
PolII_TASOR_KO2.bw
PolII_WT1.bw

PolII_WT2.bw

4. If available, provide a link to an anonymized genome browser session (e.g. UCSC).

n/a

Methodological details

5. Describe the experimental replicates.

ChIP experiments (MORC2, MPP8, TASOR, H3K9me3 and RNA PolII) were performed in two biological replicates each, with indicated antibodies. Peaks were extensively validate using ChIP-qPCR.

6. Describe the sequencing depth for each experiment.

To amplify each library we used quantitative PCR (qPCR) to endure that all libraries were amplified similarly and avoid bottlenecking of the libraries. ChIP-Seqs are pair ended, 75 bp was the read length. On average, each ChIP-seq sample contain ~40 million reads, with above 70-80% alignment.

7. Describe the antibodies used for the ChIP-seq experiments.

Rabbit MORC2 antibody (A300-149A, Bethyl Laboratories), Rabbit MPP8 antibody (16796-1-AP, Protein Technologies Inc), Rabbit TASOR antibody (HPA006735, Atlas Antibodies), Histone H3 (tri-methyl K9) antibody (ab8898, Abcam) and RNA Pol II (Santa Cruz Biotechnology, N-20 sc-899) were used in ChIP experiments.

8. Describe the peak calling parameters.

Pair-end reads were trimmed with cutadapt (-m 50 -q 10) and aligned with bowtie2 (version 2.2.9, --no-mixed --no-discordant --end-to-end -maxins 500) to the hg38 reference genome. ChIP peak calls were performed with macs2 callpeak using default settings, except for --broad flag. Background files were either ChIP input sequencing or ChIPseq from knockout cell lines for factor ChIPped.

For final list of sites MACS2 peak calls were merged, combined with 2x amount of shuffled decoy sites and read coverage for each sequencing file was obtained using bedtool coverage. Combined coverage matrix was subjected to DESeq2 procedure to reject false positives from MACS2

9. Describe the methods used to ensure data quality.

Visualization tracks were generated with bedtools genomecov (-bg -scale) with scaling factor being 10^6/number aligned reads and converted to bigWig with bedGraphToBigWig (Kent tools). BigWigs were plotted with IGV browser. Individual alignments were inspected with IGB browser. Heatmaps were generated by intersecting bam alignment files with intervals of interest (bedtools v2.25.0), followed by tabulation of the distances of the reads relative to the center of the interval and scaling to account for total aligned read numbers (10^6/number aligned). Heatmaps were plotted using a custom R function. Aggregate plots were generated by averaging rows of the heatmap matrix.

ChIP-seq repetitive sequence relationship analysis. Repeat masker was intersected with ChIP-seq peak calls to classify each masker entry as MPP8 bound, MORC2-bound or unbound. Enriched families of repeats were identified with R fisher.test() followed by FDR correction with qvalue(). Distribution of sizes of occupied vs non-occupied L1 was plotted using R density() with sizes being taken from repeat masker. ks.test() was used to reject null hypothesis that distribution of sizes for bound and unbound L1s is the same. To investigate relationship between L1 age, length and occupancy, logistic regression was performed with R glm() engine.

Quantitative analysis of H3K9me3 changes was performed by first identifying regions of significant enrichment in each sample relative to corresponding input sample (macs2 callpeak), merging the intervals into a common superset. This superset was joined with a decoy randomized set of intervals, twice the size of actual experimental interval set, with the same size distribution (bedtools shuffle). Next the read coverage was

	determined for each sample (bedtools coverage) and regions with significant change together with fold changes were identified using DESeq2 analysis paradigm. H3K9me3 regions were classified into bound vs unbound by performing intersect with MORC2 and MPP8 ChIP peak calls.
10. Describe the software used to collect and analyze the ChIP-seq data.	For ChIP-seq, we used standard and available softwares: Bowtie, MACS2, Bedtools. Details are provided in the Methods sections. All sequencing samples reported have been deposited at GEO under the accession number: GSE95374. Detailed Data and further code information are available on request from the authors.

nature research

Corresponding author(s): Joanna Wysocka and Michael Bassik

☐ Initial submission ☐ Revised version ☒ Final submission

Flow Cytometry Reporting Summary

Form fields will expand as needed. Please do not leave fields blank.

Data presentation

For all flow cytometry data, confirm that:

☒ 1. The axis labels state the marker and fluorochrome used (e.g. CD4-FITC).

☒ 2. The axis scales are clearly visible. Include numbers along axes only for bottom left plot of group (a 'group' is an analysis of identical markers).

☒ 3. All plots are contour plots with outliers or pseudocolor plots.

☒ 4. A numerical value for number of cells or percentage (with statistics) is provided.

Methodological details

5. Describe the sample preparation.	Live cells were sorted. No staining involved.
6. Identify the instrument used for data collection.	BD LSR Fortessa
7. Describe the software used to collect and analyze the flow cytometry data.	BD Diva for collection and FlowJo for analysis
8. Describe the abundance of the relevant cell populations within post-sort fractions.	The abundance of transposition positive cells is generally low. ~300,000 gated events were collected for each sample to determine GFP(+) fractions, with target of at least 200 positive cells collected.
9. Describe the gating strategy used.	Cells were gated for live/dead and doublet exclusion using FSC and SSC channels, then cells were gated for presence of mCherry signal (reporting on presence of gRNA). Events passing above gating strategy were classified as positive or negative based on SSC and GFP channel signals.

Tick this box to confirm that a figure exemplifying the gating strategy is provided in the Supplementary Information. ☒